M2-polarized macrophages prevent preterm birth and improve neonatal survival and immunity

Valeria Garcia-Flores[1,2], Zhenjie Liu[1,2], Roberto Romero[1,3,4], Yi Xu[1,2], Derek Miller[1,2], Jose Galaz[1,2,5], Andrew D. Winters[1,2], Marcelo Farias-Jofre[1,2,5], Kevin R. Theis[1,2,6], Nardhy Gomez-Lopez[1,2,6,7]

[1]Pregnancy Research Branch, Division of Obstetrics and Maternal-Fetal Medicine, Division of Intramural Research, *Eunice Kennedy Shriver* National Institute of Child Health and Human Development, National Institutes of Health, U.S. Department of Health and Human Services (NICHD/NIH/DHHS); Detroit, Michigan, and Bethesda, Maryland, USA

[2]Department of Obstetrics and Gynecology, Wayne State University School of Medicine; Detroit, Michigan, USA

[3]Department of Obstetrics and Gynecology, University of Michigan; Ann Arbor, Michigan, USA

[4]Department of Epidemiology and Biostatistics, Michigan State University; East Lansing, Michigan, USA

[5]Division of Obstetrics and Gynecology, School of Medicine, Faculty of Medicine, Pontificia Universidad Catolica de Chile; Santiago, Chile

[6]Department of Biochemistry, Microbiology, and Immunology, Wayne State University School of Medicine; Detroit, Michigan, USA

[7]Center for Molecular Medicine and Genetics, Wayne State University; Detroit, Michigan, USA

The study was conducted at the Perinatology Research Branch, NICHD/NIH/DHHS, in Detroit, Michigan; the Branch has since been renamed as the Pregnancy Research Branch, NICHD/NIH/DHHS

Correspondence: Nardhy Gomez-Lopez, PhD, Center for Molecular Medicine and Genetics, Wayne State University School of Medicine, 3236 Scott Hall, 540 E. Canfield, Detroit, Michigan 48201, USA, Tel +1 (313) 577-8904, Email: nardhy.gomez-lopez@wayne.edu; ngomezlo@med.wayne.edu, ORCID: 0000-0002-3406-5262

Conflict of interest: The authors have declared that no conflict of interest exists.

ABSTRACT

Preterm birth (PTB), commonly preceded by preterm labor, is the leading cause of neonatal morbidity and mortality worldwide. Recent advances in next-generation sequencing have revealed that most cases of preterm labor are associated with sterile intra-amniotic inflammation (SIAI), an inflammatory condition without detectable microorganisms. To date, no successful strategies to treat SIAI have been developed. Herein, we present mechanistic proof that treatment with M2-polarized macrophages (M2 MΦ) can effectively prevent SIAI-induced PTB and neonatal mortality. M2 MΦ halt the premature pathway of labor by infiltrating maternal and fetal compartments, where they inhibit NLRP3 inflammasome activation triggered by HMGB1. Furthermore, M2 MΦ dampen the HMGB1-induced inflammatory response in the amniotic cavity and fetal lung. Notably, neonates exposed to HMGB1 *in utero* display a reduced capacity to clear bacterial infection and gut microbiome dysbiosis, which are restored by M2 MΦ treatment. Our findings provide cogent evidence that M2 MΦ can serve as a cellular strategy to mitigate PTB and decrease neonatal mortality.

INTRODUCTION

Preterm birth, the leading cause of neonatal morbidity and mortality worldwide (1, 2), is often preceded by spontaneous preterm labor, a syndrome of multiple etiologies (3). Among the known and proposed causes of preterm labor, an intra-amniotic inflammatory response is the best characterized and accounts for a large proportion of cases (3-5). Intra-amniotic inflammation has been divided into two distinct clinical conditions, termed intra-amniotic infection (IAI) and sterile intra-amniotic inflammation (SIAI), both of which are characterized by elevated concentrations of inflammatory mediators such as interleukin (IL)-6 and are distinguished by the presence or absence of detectable microorganisms, respectively (6, 7). Importantly, SIAI is more prevalent than IAI in women with preterm labor and intact membranes (7) and has been linked to adverse short- and long-term outcomes for the offspring of women with this clinical condition (7, 8). Clinical studies have shown that SIAI is associated with increased amniotic fluid concentrations of alarmins or danger signals (7, 9, 10), molecules released upon cellular stress or damage (11, 12). Indeed, descriptive (7, 13) and mechanistic (14-16) studies have shown that the prototypical alarmin high-mobility group box-1 (HMGB1) participates in the initiation of a sterile intra-amniotic inflammatory response that leads to preterm delivery. Moreover, we have elucidated key signaling pathways, such as the NLRP3 inflammasome (17), that underlie the local inflammation induced by alarmins in the amniotic cavity (18-21). However, despite recent advances in the understanding of the pathophysiology of SIAI, no approved treatments that can improve maternal and neonatal outcomes currently exist, and thus there is an urgent need for the development of effective therapeutics to combat this devastating disease.

The maternal-fetal interface hosts a notable population of macrophages displaying a homeostatic or anti-inflammatory phenotype (22-29). During early gestation, these cells have been

reported to participate in implantation and placental development as well as provide local defense against potential infection (22-27, 30). In the later stages of gestation, our research was the first to propose that macrophages play a crucial and often overlooked role in maintaining pregnancy and promoting optimal fetal development (29). Specifically, we undertook mechanistic studies showing that the depletion of maternal macrophages results in preterm birth, reduces neonatal survival, and negatively impacts the growth of surviving neonates (29), providing strong evidence for the importance of these homeostatic cells for both the mother and offspring. Notably, we further demonstrated that the adoptive transfer of macrophages polarized to a homeostatic "M2-like" phenotype dampens maternal and fetal immune responses induced by intra-amniotic LPS in a model of IAI-induced preterm birth (29). It is worth considering that the intra-amniotic inflammatory response elicited by microorganisms should not be suppressed, as the host response is required for microbial clearance (31). Consequently, extant clinical findings demonstrate that the effective treatment of IAI can indeed be attained through the utilization of the bacteriostatic antibiotic clarithromycin together with other effective antibiotics to target microbes commonly detected within the amniotic cavity (32-35). Nevertheless, our pioneering study (29) provided compelling evidence supporting the use of M2 macrophages as a cellular therapy for SIAI, where careful modulation of the inflammatory response is crucial in the absence of microorganisms in the amniotic cavity. The successful use of M2 macrophages in the treatment of other human inflammatory diseases further validates this promising therapeutic approach (36-38). Hence, given the crucial role of homeostatic macrophages during late gestation, coupled with their remarkable anti-inflammatory functions, we propose that this cellular approach could represent a novel strategy for mitigating the detrimental consequences of SIAI, preventing preterm birth, and reducing its adverse neonatal outcomes.

In this study, we employed a rigorous mechanistic approach, utilizing a clinically relevant animal model of SIAI induced by the injection of HMGB1 into the amniotic cavity. Our objective was to investigate the potential of adoptively transferred M2-polarized macrophages (hereafter referred to as M2 MΦ) to prevent preterm birth and reduce adverse neonatal outcomes. To this end, we conducted tracking experiments to characterize the migration of M2 MΦ into maternal and fetal compartments. In addition, we employed molecular approaches to investigate the inflammatory response induced by HMGB1 and the anti-inflammatory effect of M2 MΦ treatment, specifically targeting those involved in the common pathway of parturition. We also performed bacterial challenges on neonates born to dams with SIAI and in those that received M2 MΦ treatment to evaluate their immunocompetence. Finally, we compared the structure of the neonatal gut microbiome and examined immune response-related transcripts between the offspring of treated and untreated dams. Collectively, our data indicate that adoptive transfer of M2 MΦ may represent a novel cellular approach to prevent preterm birth and ameliorate the adverse effects of SIAI on neonatal wellbeing.

RESULTS

Treatment with M2-polarized macrophages prevents preterm birth and neonatal mortality induced by intra-amniotic HMGB1

Women with preterm labor and SIAI have elevated amniotic fluid concentrations of alarmins such as HMGB1 (7, 9, 10). To mimic the human disease, pregnant mice underwent an ultrasound-guided intra-amniotic injection of HMGB1 (Figure 1A). Intra-amniotic delivery of HMGB1 induced preterm birth in a subset of mice (Figure 1B), as reflected by the shortened gestational length (Figure 1C). Importantly, the adoptive transfer of M2 MΦ drastically reduced the preterm birth rate (Figure 1B), increasing gestational length (Figure 1C). Moreover, M2 MΦ treatment improved the neonatal survival rate across the first three weeks of life, which was similar to that of control neonates (Figure 1D). Neonatal weight, which was reduced in the first three weeks of life upon intra-amniotic delivery of HMGB1, was consistently increased in neonates born to dams that received M2 MΦ treatment (Figure 1E-G). To investigate whether HMGB1 had adverse effects in neonatal life due to fetal compromise, which could be rescued by M2 MΦ treatment, we assessed fetal wellbeing using Doppler ultrasound and biometric parameters. Intra-amniotic delivery of HMGB1 did not significantly alter the fetal heart rate and peak systolic velocity (PSV) (Figure 1H&I), nor did it affect the fetal:placental weight ratio (Figure 1J), suggesting that the inflammatory response triggered by this alarmin does not induce sonographically detectable fetal compromise, as is observed in dams intra-amniotically injected with microbial products that initiate a stronger cytokine response (39). Consequently, the fetal:placental weight ratio remained consistent upon M2 MΦ treatment (Figure 1K). Taken together, these data indicate that M2 MΦ treatment can prevent HMGB1-induced preterm birth and the resulting adverse neonatal outcomes.

Adoptively-transferred M2 macrophages reach maternal compartments and the maternal-fetal interface

Next, to evaluate the kinetics of adoptively transferred M2 MΦ, we utilized a model wherein M2 MΦ derived from donor CD45.1^{+} mice were transferred to recipient CD45.2^{+} dams injected with HMGB1 (Figure 2A). Afterwards, maternal blood as well as maternal and fetal tissues were collected to track the migration of transferred cells based on the representative gating shown in Figure 2B. M2 MΦ were present in the maternal blood at 2 h post-injection and diminished at later time points (Figure 2C). M2 MΦ were also detected in the maternal lung at lower proportions than the blood and were similarly diminished over time (Figure 2D). A noteworthy, albeit small fraction of M2 MΦ was detected in the uterus (Figure 2E) and the decidua (Figure 2F). While the uterine M2 MΦ fraction increased over time (Figure 2E), the decidual M2 MΦ fraction remained stable (Figure 2F). Interestingly, the placental M2 MΦ fraction was comparable at 2 h and 6 h post-injection; yet, a sudden drop was observed at 12 h (Figure 2G), resembling the M2 MΦ dynamics in the maternal blood at this timepoint. M2 MΦ were neither detected in the fetal membranes nor in the amniotic fluid of recipient mice (Figure 2H&I). Moreover, few or no donor M2 MΦ were detected in other fetal tissues (fetal intestine, fetal lung, and fetal liver) at each time point (Supplementary Figure 1). Therefore, these data demonstrate that adoptively transferred M2 MΦ can reach maternal compartments and the maternal-fetal interface, where they display distinct dynamics over time, but do not appear to reach the fetal tissues and amniotic cavity.

M2 macrophages dampen HMGB1-induced intra-amniotic inflammation and inflammasome activation in the amniotic cavity

First, we investigated whether preterm birth induced by intra-amniotic HMGB1 was accompanied by an inflammatory response in the amniotic cavity, and whether this could be prevented by M2 MΦ treatment. Hence, we collected the amniotic fluid of HMGB1-injected dams at 24, 48, 72, or 96 h post-injection to evaluate the concentrations of classic cytokines associated with SIAI (9, 10) (Figure 3A). Intra-amniotic delivery of HMGB1 increased the amniotic fluid concentrations of IL-6 at 72 h post-injection (Figure 3B), whereas the concentrations of IL-1β and TNF were not strongly affected (Supplementary Figure 2). Notably, M2 MΦ treatment not only reduced amniotic fluid concentrations of IL-6 at 72 h post-injection, but also those of TNF and IL-1β (Figure 3C&D).

The NLRP3 inflammasome is a key signaling pathway implicated in the intra-amniotic inflammatory response leading to preterm labor and birth (40-42). Our prior human and murine studies showed that SIAI is linked to the activation of the NLRP3 inflammasome in the amniotic cavity (21, 41). Therefore, we next determined whether M2 MΦ treatment could inhibit inflammasome activation in the amniotic cavity. Intra-amniotic delivery of HMGB1 caused an increase in active CASP-1 and mature IL-1β in amniotic fluid as determined by immunoblotting (Figure 3E-G). Notably, M2 MΦ treatment dampened such inflammasome activation by reducing both active CASP-1 and mature IL-1β (Figure 3H-J).

Taken together, these data indicate that adoptively transferred M2 MΦ can exert their homeostatic effects in the amniotic cavity by dampening HMGB1-induced inflammatory cytokine release and by inhibiting inflammasome activation, a critical pathway in the preterm labor cascade (17).

M2 macrophages dampen inflammasome activation and regulate gene expression in maternal-fetal tissues participating in the pathway of premature labor

The processes of term and preterm labor share a common underlying pathway including uterine contractility, cervical remodeling, and fetal membrane/decidual activation (43-46). A key characteristic of preterm labor is the activation of pro-inflammatory signaling networks such as the NLRP3 inflammasome in the uterine tissues and fetal membranes, but not in the decidua or cervix (18, 21, 39, 41, 47, 48); therefore, we determined whether M2 MΦ treatment prevents preterm birth by modulating inflammasome activation in the uterus (Figure 4A) and fetal membranes (Figure 5A). Intra-amniotic delivery of HMGB1 induced increased levels of active CASP-1 and mature IL-1β in the uterine tissues (Figure 4B-E). M2 MΦ treatment resulted in modest dampening of inflammasome activation, as evidenced by the tendency for reduced active CASP-1 and mature IL-1β (Figure 4F-J). Neither HMGB1 alone nor treatment with M2 MΦs modified the uterine expression of transcripts associated with contractility or non-inflammasome immune mediators (Supplementary Figure 3), which are linked to myometrial activation (49-51). The data presented in this study provides further evidence to support the notion that inhibition of the inflammasome alone can effectively prevent preterm labor and birth induced by SIAI (18, 21).

Intra-amniotic delivery of HMGB1 induced a similar response in the fetal membranes as observed in the uterine tissues, with increased levels of active CASP-1 and mature IL-1β indicating the activation of inflammasome (Figure 5B&C). Moreover, the expression of *Ccl17* in the fetal membranes was increased upon intra-amniotic delivery of HMGB1 together with a tendency for elevated expression of other inflammation-associated genes and inflammatory mediators (Figure 5D). Importantly, M2 MΦ treatment not only abrogated inflammasome activation, as indicated by

reduced active CASP-1 and mature IL-1β (Figure 5E&F), but also caused downregulation of various other inflammatory genes (Figure 5G). Intra-amniotic delivery of HMGB1 did not induce drastic changes in inflammatory gene expression in the decidua; yet, treatment with M2 MΦ reduced the expression of several transcripts in this maternal-fetal interface (Supplementary Figure 4A&B), suggesting that these homeostatic cells can exert anti-inflammatory effects even in the absence of a heightened inflammatory response.

Collectively, these data indicate that M2 MΦ exert immunomodulatory effects in key tissues participating in the common pathway of labor, including the dampening of NLRP3 inflammasome activation in the uterus and fetal membranes, providing a potential mechanism whereby this cellular therapy halts HMGB1-induced premature labor and thereby prevents preterm birth.

M2 macrophages modulate placental and fetal inflammation caused by intra-amniotic delivery of HMGB1

Given our finding that adoptively transferred M2 MΦ could reach the placenta, we next determined whether such immune cells could also exert homeostatic effects in this fetal organ and the fetus itself following the intra-amniotic delivery of HMGB1. The placenta was collected to evaluate inflammatory gene expression, revealing that intra-amniotic delivery of HMGB1 triggered the upregulation of *Tlr4*, *Gja1*, and *Ptgs2* as well as a tendency for increased expression of *Tnf*, *Tnfrsf1a*, and *Nfkb2* in this compartment (Supplementary Figure 5A). Notably, administration of M2 MΦ downregulated the expression of *Ccl17* and *Nfkb2* as well as tended to dampen the expression of *Tlr4*, *Tnf*, *Tnfrsf1a*, *Gja1*, and *Ptgs2* in the placenta (Supplementary Figure 5B). In the fetal lung (Figure 6A), intra-amniotic delivery of HMGB1 upregulated the

expression of genes associated with inflammation and inflammasome activation, such as *Il6*, *Tnfrsf1a*, *Il33*, *Nlrp6*, and *Tlr9* (Figure 6B&C). Similar to the placenta, M2 MΦ treatment downregulated the expression of *Tnfrsf1a* and *Nod1* as well as tended to dampen *Il6*, *Il33*, *Nlrp6*, *Aim2*, *Tlr9*, and *Ccl22* in the fetal lung, thereby demonstrating effectiveness in major fetal organs (Figure 6D&E). Hence, the above data indicate that M2 MΦ can help to regulate fetal inflammation triggered by intra-amniotic delivery of HMGB1, suggesting that this treatment could have beneficial effects *in utero* that could extend into neonatal life.

Prenatal M2 macrophage treatment improves neonatal immunocompetence following *in utero* exposure to HMGB1

To determine whether neonatal survival was improved merely by the extension of gestational length resulting in term delivery, or by direct effects of the M2 MΦ treatment, we first examined the survival rates of neonates exposed to intra-amniotic HMGB1 with or without M2 MΦ treatment. Strikingly, neonates exposed to intra-amniotic HMGB1 and born at term displayed diminished survival (42%) compared to those exposed to HMGB1 that received M2 MΦ treatment (66%) (Figure 7A). We then evaluated the immunocompetence of control neonates (i.e., pups born to dams without any treatment) and neonates exposed *in utero* to HMGB1 alone, HMGB1 with vehicle treatment, or HMGB1 with M2 MΦ treatment by performing intraperitoneal injection of group B *Streptococcus* (GBS) at two weeks of age (Figure 7B). *In utero* exposure to HMGB1 caused low neonatal survival rates within the first five days post-GBS infection (Figure 7C). Notably, prenatal M2 MΦ treatment improved neonatal survival to be comparable to controls (Figure 7C), indicating improved immunocompetence. HMGB1 *in utero* exposure also negatively impacted neonatal weight, which was significantly reduced compared to controls at five days post-

infection (Figure 7D). Prenatal M2 MΦ treatment partially rescued neonatal weight but did not fully restore it to the control trajectory (Figure 7D). The improved neonatal survival and weight driven by prenatal M2 MΦ treatment were accompanied by reduced incidence of hypothermia [considered the murine equivalent of fever (52, 53)] upon GBS infection (Supplementary Figure 6A&B). Next, to uncover the molecular changes underlying such improved immunocompetence, we evaluated gene expression in the neonatal intestine (i.e., the small intestine, cecum, and colon) and lung (Figure 7E). Prenatal M2 MΦ treatment was associated with the enhanced expression of inflammatory mediators and markers in the neonatal small intestine (Figure 7F&G). Consistent changes were observed in the cecum and colon, indicating bolstered neonatal defense after prenatal M2 MΦ treatment (Figure 7H-K). An opposite effect was observed in the neonatal lung, where the inflammatory response was dampened in neonates that received prenatal M2 MΦ treatment (Supplementary Figure 6C). Taken together, these data provide evidence that prenatal M2 MΦ treatment bolsters immunocompetence and promotes a healthy inflammatory response to infection in neonates exposed to HMGB1-induced inflammation *in utero*.

Prenatal M2 macrophage treatment ameliorates neonatal gut dysbiosis driven by *in utero* exposure to HMGB1

Prenatal M2 MΦ treatment altered the neonatal gut transcriptomic profile; therefore, we last investigated whether *in utero* exposure to HMGB1 affected the neonatal gut microbiome and whether such changes could be reverted. We performed 16S rRNA gene sequencing of the neonatal small intestine, cecum, and colon from dams injected with HMGB1 with or without M2 MΦ treatment (Figure 8A). Principal coordinate analysis (PCoA) revealed that the tissue microbiomes were strongly clustered by treatment group (Supplementary Figure 7A) and underwent consistent

changes in structure upon HMGB1 or M2 MΦ treatment (Supplementary Figure 7B). In the small intestine, M2 MΦ treatment was associated with a shift in the microbiome structure (Figure 8B&C and Supplementary Figure 7C) characterized by decreased abundance of *Rodentibacter* (ASV-5) and *Ruminiclostridium* (ASV-17) (Figure 8D and Supplementary Figure 7D). Similar trends were also observed in the cecum (Figure 8E&F and Supplementary Figure 7E), in which decreased abundance of *Ruminiclostridium* (ASV-17), Lachnospiraceae (ASV-24), and *Lachnoclostrium* (ASV-15) was observed together with increased Lachnospiraceae (ASV-39) (Figure 8G and Supplementary Figure 7F). Consistently, in the colon the microbiome structure was altered by HMGB1 and modified by M2 MΦ treatment (Figure 8H&I and Supplementary Figure 7G), resulting in decreased abundance of *Ruminiclostridium* (ASV-17), Lachnospiraceae (ASV-24), and *Lachnoclostrium* (ASV-15) (Figure 8J and Supplementary Figure 7H). Overall, these data indicate that M2 MΦ treatment can alleviate the adverse effects of *in utero* exposure to HMGB1-induced intra-amniotic inflammation on the neonatal microbiome.

DISCUSSION

In the current study, we provide mechanistic evidence for M2 MΦ treatment as a cellular therapy that can prevent preterm birth induced by the intra-amniotic injection of the prototypical alarmin HMGB1, which is implicated in SIAI (7, 13-16). The lack of knowledge regarding specific molecular targets in women with SIAI has made the investigation of useful treatment options significantly more challenging. Our current data point to several potential mechanisms whereby the adoptive transfer of M2 MΦ is preventing preterm birth. First, prior studies have indicated that physiologic and pathologic labor is accompanied by a shift in macrophage polarization, primarily at the maternal-fetal interface, wherein a subset of such cells acquires a pro-inflammatory M1-like phenotype (28, 29). Given that adoptively transferred M2 MΦ were shown to reach the maternal-fetal interface herein, it is possible that such cells help to maintain a predominance of homeostatic macrophages in this compartment and thereby dampen inflammatory signaling that could trigger the premature onset of labor. Second, labor involves a coordinated process of activation across multiple maternal and gestational tissues, conventionally referred to as the common pathway of parturition (3, 44, 45), that includes modulation of gene expression related to contractility, tissue remodeling (e.g., matrix metalloproteinases), and inflammation (48, 50, 51, 54-57). Adoptively transferred M2 MΦ may help to bolster the homeostatic functions of resident maternal cells and prevent the premature initiation of labor-associated transcriptional changes. The latter concept is supported by our prior observations that the depletion of maternal MΦ can result in preterm birth, implicating these cells in pregnancy maintenance (29). M2 MΦ are known to express immunomodulatory factors such as arginase-1 and can modify the tissue microenvironment, thereby preventing local immune activation (58, 59). Third, we previously demonstrated that the inflammasome is a key pathway involved in premature labor induced by microbes (39, 47) or

alarmins (18, 19, 21, 60). Indeed, as a proof of concept, we administered a specific inhibitor of the NLRP3 inflammasome (i.e., MCC950) (61) to dams injected with the alarmin S100B and observed reduced rates of preterm birth and adverse neonatal outcomes (18). Despite the potential benefits of NLRP3 inhibitors, more research is necessary to fully understand their impact on maternal and fetal safety before recommendation for use during pregnancy. Herein, we show that M2 MΦ exert their effects by dampening inflammasome activation in the uterine tissues and fetal membranes, thereby providing an alternative approach to the direct targeting of the NLRP3 molecule to block this signaling pathway. Together, the above data provide evidence that the adoptive transfer of M2 MΦ may induce a sufficient immunomodulatory signal to overcome pro-labor signaling driven by HMGB1-induced intra-amniotic inflammation, thereby preventing premature labor leading to preterm birth.

Herein, we also showed that prenatal M2 MΦ treatment reduced HGMB1-driven inflammatory responses in the fetal compartment; namely, the amniotic cavity (amniotic fluid, placenta, and fetal membranes) and the fetus itself. Interestingly, our tracking experiments indicated that adoptively transferred M2 MΦ did not appear to enter the amniotic cavity or fetal organs (i.e., intestine, lung, and liver), as opposed to the maternal reproductive tissues, maternal-fetal interface, and placenta, suggesting that this treatment could be safely utilized in pregnant women. These observations point to the indirect regulation of fetal inflammatory responses by M2 MΦ cells, likely through the release of soluble mediators. M2 MΦ specifically have been shown to release a wide array of factors including not only conventional cytokines/chemokines such as IL-10 but also growth factors, neurotransmitters, hormones, and lipid metabolites (59, 62). The enhanced numbers of M2 MΦ present in the maternal circulation and tissues may result in transiently elevated concentrations of such factors, which can then be transmitted across the

maternal-fetal interface into the amniotic cavity and potentially the fetus, as has been demonstrated for multiple cytokines (63-67). The prolonged dampening of inflammatory gene expression in the placenta and fetal organs by M2 MΦ may not only protect the fetus against the adverse effects of such inflammation but may also promote continued fetal growth. Indeed, in a previous investigation we showed that the loss of another maternal homeostatic cell type, regulatory T cells, negatively impacted the placental expression of transcripts enriched for developmental and cellular processes (68). Although the current study did not include a high-throughput screen of placental gene expression, our data support a similar role for maternal homeostatic macrophages in promoting fetal development and protecting against the adverse effects of alarmin-induced inflammation in the amniotic cavity.

Sterile intra-amniotic inflammation is not only detrimental in terms of short-term outcomes, such as preterm birth, but is importantly linked to long-term negative consequences for the offspring as indicated by human data (7, 8) and animal studies (14-16, 18, 19, 60). Such consequences are not entirely the result of prematurity, as neonates born at term to HMGB1-injected dams still had reduced survival compared to those that received M2 MΦ treatment. Thus, even a relatively brief exposure to alarmin-induced intra-amniotic inflammation imprints fetal changes that can be carried over to neonatal life, independently of gestational age at delivery. This concept is supported by previous research demonstrating that prenatal treatments or exposures during gestation can induce permanent changes in neonatal life (69-71). A pioneering study utilized a model of transient maternal microbial colonization during pregnancy to demonstrate changes in immune cell composition and gene expression in the neonatal intestine as well as improved neonatal resistance to bacterial challenge (69). The above report indicated that antibody-mediated transfer of microbial products from the mother to the fetus may occur, thereby initiating

a chain of immune events leading to the observed neonatal phenotype (69). Yet, in the current model of M2 MΦ treatment, it is unlikely that maternal antibodies are primary mediators of the beneficial effects on neonatal immunocompetence, given that most macrophage-derived mediators (e.g., cytokines) should not require antibody shuttling to reach the fetal compartment (63-67). Another study utilized a similar model of transient gestational infection to demonstrate the involvement of an IL-6/Th17 axis in promoting enhanced resistance to gut infection in the neonates (70), suggesting that prenatal immunological events can imprint lasting changes on the offspring through multiple mechanisms. Transient exposure to a maternally-derived inflammatory cytokine, IL-6, was similarly explored in pregnant mice and found to result in permanent alteration of neuronal gene programs, providing mechanistic evidence for how prenatal inflammation drives long-term changes in neonatal neurodevelopment (71). Strikingly, in the current study we found that maternal M2 MΦ treatment largely abrogated the adverse outcomes driven by intra-amniotic inflammation by restoring neonatal survival and improving weight gain following bacterial challenge. Similar to the abovementioned study of the neonatal brain (71), altered expression of relevant genes (e.g., related to host defense) was observed in the neonatal gastrointestinal (GI) tract and lung, indicating the far-reaching effects of maternal M2 MΦ treatment in the neonate. Therefore, the current study supports two key concepts: first, that acute insults during fetal life can alter developmental programming leading to impaired immunocompetence in adolescence/adulthood, the full extent and importance of which are still poorly understood; second, that the cellular therapy using M2 MΦ demonstrated herein exerts sufficient homeostatic effects to significantly counteract such changes.

Proper formation of the gut microbiota during early life is essential for the development of a healthy adult GI tract (72). Indeed, multiple inflammatory, metabolic, neurologic, cardiovascular,

and GI diseases have been linked to disruption of the microbiota during this time (73). Importantly, the risk of gut dysbiosis is increased in preterm neonates compared to those delivered at term (72), and thus the prevention or treatment of premature labor leading to preterm birth, particularly in the context of inflammatory conditions such as SIAI, is essential to ensure the development of a healthy gut microbiota and avoid long-term consequences. Several prenatal events have been studied and found to contribute to microbiota dysbiosis in human neonates, including maternal diet, antibiotic use, and the presence of placental acute histologic lesions (i.e., acute chorioamnionitis and funisitis) (72, 74). Specifically, the combined presence of acute chorioamnionitis/funisitis was linked to altered microbial composition in neonatal fecal samples, including modified abundance of *Bacteroidetes* and *Fusobacteria* (75). Importantly, neonates affected by acute chorioamnionitis alone or acute chorioamnionitis/funisitis had higher incidence of late-onset sepsis/death, thereby providing an association between microbiome alterations and both short-term adverse events (75) and long-term consequences (73). Consistent with these studies, herein we demonstrated that the adverse neonatal outcomes driven by *in utero* exposure to alarmins are similarly associated with alterations of the gut microbiome composition, and that gestational M2 MΦ treatment seemed to negate such changes. Although the current study did not follow neonates past the first three weeks of life, these observations suggest that M2 MΦ treatment can promote the maturation of a "normal" gut microbiota that can lead to reduced disease risk in adulthood.

Collectively, the data presented herein provide substantial evidence of a functional role for homeostatic M2-polarized MΦ in preventing preterm birth and adverse neonatal outcomes driven by HMGB1-induced intra-amniotic inflammation, a model that resembles the clinical scenario of SIAI-associated preterm labor and birth. Specifically, adoptively transferred M2 MΦ migrate to

maternal reproductive tissues and the maternal-fetal interface, where these cells dampen key inflammatory signaling pathways, such as the NLRP3 inflammasome, and prevent activation of key processes in the common pathway of labor, thereby extending gestational length. Importantly, the homeostatic functions of M2 MΦ extend to the placenta, fetus, and amniotic cavity, consistently downregulating inflammatory gene expression and diminishing cytokine release. Such diminished exposure of the fetus to intra-amniotic inflammation results in beneficial effects during neonatal life; namely, improved neonatal capacity to clear bacterial infection and restoration of the dysregulated gut microbiome. In conclusion, these findings provide strong mechanistic evidence that M2 MΦ can serve as a cellular approach to not only prevent SIAI-associated premature labor leading to preterm birth but to also improve neonatal quality of life, including immunity, following *in utero* exposure to inflammation.

METHODS

Mice

C57BL/6 (strain # 000664) and B6 CD45.1 (B6.SJL-*Ptprc*^{a} *Pepc*^{b}/BoyJ; strain # 002014) mice were purchased from The Jackson Laboratory (Bar Harbor, ME, USA). Mice were housed in the animal care facility at the C.S. Mott Center for Human Growth and Development at Wayne State University (Detroit, MI, USA) under a circadian cycle (light:dark = 12:12 h). Eight- to twelve-week-old females were mated with males of proven fertility. Females were checked daily between 8 and 9 a.m. to investigate the appearance of a vaginal plug, which indicated 0.5 days *post coitum* (dpc). Plugged females were then housed separately from the male mice and their weights were monitored daily. A weight gain of ≥ 2 grams by 12.5 dpc confirmed pregnancy. Mice were randomly assigned to study groups prior to the experiments described herein. Numbers of biological replicates are indicated in each figure caption.

Intra-amniotic administration of HMGB1

Ultrasound-guided intra-amniotic injection of HMGB1 was performed as previously reported (14-16). Briefly, dams were anesthetized on 14.5 dpc by inhalation of 2% isoflurane (Fluriso^{TM}/Isoflurane, USP; VetOne, Boise, ID, USA) and 1–2 L/min of oxygen in an induction chamber, and a mixture of 1.5–2% isoflurane and 1.5–2 L/min of oxygen was used to maintain anesthesia. Mice were positioned on a heating pad and stabilized with adhesive tape, and fur was removed from the abdomen and thorax using Nair cream (Church & Dwight Co., Inc., Ewing, NJ, USA). Body temperature was detected with a rectal probe (VisualSonics, Toronto, ON, Canada) throughout the procedure, and respiratory and heart rates were monitored by electrodes embedded in the heating pad. An ultrasound probe was fixed and mobilized with a mechanical holder, and

the transducer was slowly moved toward the abdomen (76). The ultrasound-guided intra-amniotic injection of recombinant human HMGB1 (Biolegend, San Diego, CA, USA) at a concentration of 9 ng dissolved in 100 μL of sterile 1X phosphate-buffered saline (PBS; Life Technologies, Grand Island, NY, USA) was performed in each amniotic sac using a 30G needle (BD PrecisionGlide Needle; Becton Dickinson, Franklin Lakes, NJ, USA). After ultrasound completion, mice were placed under a heat lamp for recovery defined as when the mouse resumed normal activities, such as walking and interacting with its environment, which typically occurred within 10 min after removal from anesthesia. After recovery, dams were monitored via video camera (Sony Corporation, Tokyo, Japan) to observe pregnancy and neonatal outcomes.

Isolation, differentiation, and adoptive transfer of M2-polarized macrophages

Bone marrow cells were isolated, differentiated, and adoptively transferred following a previously established protocol (29). Briefly, bone marrow cells were collected from female mice (12-16 weeks old) and treated with red blood cell lysis buffer (Ammonium Chloride Solution; Cat# 07800, Stem Cell Technologies; Vancouver, CA). Then, cells were resuspended and cultured in Iscove's Modified Dulbecco's Media (IMDM) medium (Thermo-Fisher Scientific; Waltham, MA, USA) supplemented with 10% fetal bovine serum (FBS; Invitrogen, Carlsbad, CA, USA), 1X antibiotic-antimycotic (Cat# 15240062; Thermo-Fisher Scientific), and 10 ng/mL recombinant macrophage colony-stimulating factor (M-CSF; Cat# 576402; BioLegend, San Diego, CA, USA) for 7 days. On day 7, the culture medium was replaced with fresh IMDM medium supplemented with 10% FBS, 1X antibiotic-antimycotic, 10 ng/mL of recombinant IL-4 (Cat# 574302, BioLegend), and 10 ng/mL of recombinant IL-13 (Cat# 575902, BioLegend). After 14-18 h, M2 MΦ were collected by washing with ice-cold phosphate-buffered saline (PBS; Fisher Scientific

Bioreagents, Fair Lawn, NJ, USA or Life Technologies Limited, Pailey, UK). Approximately 2-5 x 10^6 cells were resuspended in 100 µL 1X PBS for intravenous injection into dams on 13.5 and 14.5 dpc, prior to the administration of HMGB1 or PBS on 14.5 dpc.

Perinatal outcomes

Gestational length was calculated as the duration of time from the presence of the vaginal plug (0.5 dpc) to the detection of the first pup in the cage bedding. Preterm birth was defined as delivery occurring before 18.75 dpc based on the lowest gestational age at delivery observed in the control group. The rate of preterm birth was calculated as the proportion of females delivering preterm out of the total number of mice per group. The rate of stillbirth was defined as the proportion of delivered pups found dead among the total number of pups. The rate of neonatal mortality was defined as the proportion of pups found dead among the total number of pups. Neonatal mortality rates and weights were calculated and recorded at postnatal weeks 1, 2, and 3.

Evaluation of maternal-fetal obstetrical parameters by ultrasonography

Pregnant C57BL/6 mice were intra-amniotically injected with 9 ng of HMGB1/100 µL of PBS (or 100 µL 1x PBS as control) in each amniotic sac on 14.5 dpc and maternal-fetal obstetrical parameters were evaluated by ultrasonography (VisualSonics Inc.) 96 h after, as previously described (68, 76-80). The fetal heart rate and the peak systolic velocity (PSV) of the umbilical arteries of three to four fetuses from each dam were examined.

Tracking transferred M2-polarized macrophages *in vivo*

Bone marrow from B6 CD45.1 mice was collected, isolated, and differentiated into M2 MΦ as described above. Pregnant C57BL/6 recipient mice were intravenously injected with 2-5x10^6 CD45.1+ donor M2 MΦ at 13.5 and 14.5 dpc followed by intra-amniotic injection of HMGB1 on 14.5 dpc, as described above. Mice were euthanized at 2, 6, or 12 h after intra-amniotic injection to collect the maternal blood, maternal lung, uterus, decidua, and placenta as well as the fetal membrane, fetal intestine, fetal liver, fetal liver, and amniotic fluid. Whole maternal blood (100 µL) was used directly for immunophenotyping following the procedure described below. For maternal and fetal tissues, leukocytes were isolated by following protocols adapted from (81). Briefly, maternal and fetal tissues were gently minced using fine scissors and enzymatically digested with StemPro Accutase Cell Dissociation Reagent (Cat# A1110501, Thermo-Fisher) for 30 min at 37°C. Cells were filtered using a 100 µm cell strainer (Cat# 22-363-549, Fisher Scientific, Fair Lawn, NY, USA) followed by washing with 1X PBS prior to immunophenotyping. Immediately after isolation of leukocytes, cell pellets were re-suspended in FACS buffer and pre-incubated with rat anti-mouse CD16/CD32 Fc Block™ (Cat# 553142, clone 2.4G2; BD Bioscience, Franklin Lakes, NJ, USA) for 10 min on ice and subsequently incubated with specific fluorochrome-conjugated monoclonal anti-mouse antibodies shown in Supplementary Table 1. Cells were acquired using the BD LSRFortessa flow cytometer (BD Biosciences) with FACSDiva 9.0 software (BD Biosciences). CountBright absolute counting beads (Thermo Fisher Scientific) were added prior to acquisition. The analysis was performed and the figures were created by using FlowJo software version 10 (FlowJo, Ashland, OR, USA).

Tissue collection from dams intra-amniotically injected with HMGB1

Dams were euthanized at 24, 48, 72, and 96 h after intra-amniotic HMGB1 injection for tissue collection. The amniotic fluid was collected from each amniotic sac and centrifuged at 1,300 x g for 5 min at 4°C. The resulting supernatants were stored at -20°C until analysis. The maternal whole blood was collected from each dam, mixed with heparin (Cat# 2106-15VL; Sigma-Aldrich, St. Louis, MO, USA), and centrifuged at 800 x g for 10 min at 4°C. Tissue collection of the uterus, decidua, placenta, fetal membrane, and fetal lung was performed. The placentas and fetuses were imaged and weighed during tissue dissection. The collected tissues were snap-frozen in liquid nitrogen for immunoblotting or preserved in RNA*later* Stabilization Solution (Cat# AM7021; Invitrogen by Thermo-Fisher Scientific, Carlsbad, CA, USA), according to the manufacturer's instructions.

Determination of cytokine concentrations in amniotic fluid

Concentrations of IL-6, IL-1β, and TNF were determined in the amniotic fluid using the U-PLEX Custom Biomarker Group 1 (ms) assay (Cat# K15069M-2; Meso Scale Discovery, Rockville, MD, USA), according to the manufacturer's instructions. Plates were read using the MESO QuickPlex SQ 120 (Meso Scale Discovery) and analyte concentrations were calculated using the Discovery Workbench software version 4.0 (Meso Scale Discovery). The sensitivities of IL-6, IL-1β, and TNF were 4.8 pg/mL, 3.1 pg/mL, and 1.3 pg/mL, respectively.

RNA isolation, cDNA synthesis, and qPCR analysis of murine tissues

Total RNA was isolated from the uterus, decidua, placenta, fetal membranes, fetal lung, neonatal lung, neonatal small intestine, neonatal cecum, and neonatal colon (see below for neonatal immunocompetence experiments) using QIAshredders (Cat# 79656; Qiagen, Germantown, MD,

USA), RNase-Free DNase Sets (Cat# 79254; Qiagen), and RNeasy Mini Kits (Cat# 74106; Qiagen), according to the manufacturer's instructions. The NanoDrop 8000 spectrophotometer (Thermo Scientific, Wilmington, DE, USA) and the Bioanalyzer 2100 (Agilent Technologies, Waldbronn, Germany) were used to evaluate RNA concentrations, purity, and integrity. SuperScript IV VILO Master Mix (cat# 11756050; Invitrogen by Thermo Fisher Scientific Baltics UAB, Vilnius, Lithuania) was used to synthesize complementary (c)DNA. Gene expression profiling of the tissues was performed on the BioMark System for high-throughput qPCR (Fluidigm, San Francisco, CA, USA) with the TaqMan gene expression assays (Applied Biosystems, Life Technologies Corporation, Pleasanton, CA, USA) listed in Supplementary Table 2. Negative delta cycle threshold ($-\Delta C_T$) values were determined using multiple reference genes (*Actb*, *Gapdh*, *Gusb*, and *Hsp90ab1*) averaged within each sample for contractility-associated and inflammatory genes. The $-\Delta C_T$ values were normalized by calculating the Z-score of each gene with the study groups. Heatmaps were created representing the Z-score of each $-\Delta C_T$ using GraphPad Prism (GraphPad, San Diego, CA, USA).

Protein isolation from murine tissues

Snap-frozen fetal membrane and uterus were mechanically homogenized in 1x PBS containing a complete protease inhibitor cocktail (Cat# 11836170001; Roche Applied Sciences, Mannheim, Germany) for 10 min. The resulting lysates were centrifuged at 16,100 x g (maximum speed) for 5 min at 4°C. The total protein concentrations in amniotic fluid (supernatant) and tissue lysate samples were tested by the Pierce BCA Protein Assay Kit (Cat# 23225; Pierce Biotechnology, Thermo-Fisher Scientific, Inc., Rockford, IL, USA) prior to immunoblotting. Cell lysates or concentrated culture medium from murine bone marrow-derived macrophages were

utilized as positive controls for the expression of active CASP-1 and mature IL-1β, as previously described (39).

Western blotting of amniotic fluid and murine tissues

Cell lysates or culture supernatants from murine bone marrow-derived macrophages (30 μg per well; positive control), amniotic fluid (20 μg total protein per well), fetal membrane lysates (75 μg per well), and uterine tissue lysates (75 μg per well) were subjected to electrophoresis in sulfate-polyacrylamide gels (Cat# NP0336BOX; Invitrogen). The proteins were transferred onto nitrocellulose membranes (Cat# 1620145; Bio-Rad, Hercules, CA, USA), which were then submerged in 5% blotting-graded blocking solution (Cat# 1706404; Bio-Rad) for 30 min at room temperature. Next, the membranes were probed overnight at 4°C with anti-mouse CASP-1 (Cat# 14-9832-82; Thermo-Fisher Scientific) or anti-mouse mature IL-1β (Cat# 63124S; Cell Signaling Technology, Danvers, MA, USA; only for fetal membranes). After incubation with each primary antibody, membranes were incubated with HRP-conjugated anti-rat IgG (Cat# 7077S; Cell Signaling) for CASP-1 or HRP-conjugated anti-heavy chain of rabbit IgG (Cat# HRP-66467; Proteintech, Rosemont, IL, USA) for mature IL-1β for 1 h at room temperature. The ChemiGlow West Chemiluminescence Substrate Kit (Cat# 60-12596-00; ProteinSimple, San Jose, CA, USA) was used to detect chemiluminescence signals, and corresponding images were acquired using the ChemiDoc Imaging System (Bio-Rad). The membranes that were loaded with fetal membrane and uterine tissue lysates were re-probed for 1 h at room temperature with a mouse anti-β-actin (ACTB) monoclonal antibody (Cat# A5441, Sigma-Aldrich). Then, the membranes were incubated with HRP-conjugated anti-mouse IgG (Cat# 7076S; Cell Signaling) for 30 min at room temperature. The chemiluminescence signals of the ACTB were detected as shown above. Finally,

quantification was performed using ImageJ software as previously reported (39). In short, each individual protein band was automatically quantified on the blot images. The internal control, β-actin, was used to normalize the target protein expression in each fetal membrane and uterine tissue sample for relative quantification.

Immunoprecipitation of mature IL-1β in amniotic fluid and uterine tissues

Immunoprecipitation of cleaved IL-1β from uterine tissue lysates and amniotic fluid was performed using the Pierce™ Classic IP Kit (Cat# 26146; Thermo Fisher Scientific) following the manufacturer's instructions. Amniotic fluid samples (n = 3 per study group) were pooled. Culture supernatants from murine bone marrow-derived macrophages were utilized as positive controls. Each uterine tissue lysate (1 mg protein) or pooled amniotic fluid sample (1 mg protein) was pre-cleared using the control agarose resin and incubated with rabbit anti-mouse mature IL-1β antibody overnight at 4°C to form the immune complex. Next, the immune complex was captured using Pierce Protein A/G Agarose. After several washes to remove non-bound proteins, the immune complex was eluted with sample buffer and subjected to electrophoresis in 4%–12% polyacrylamide gels followed by Western blot transfer, as described above. The blot was then incubated with rabbit anti-mouse mature IL-1β antibody, followed by incubation with an HRP-conjugated anti-heavy chain of rabbit IgG antibody. Finally, chemiluminescence signals were detected with the ChemiGlow West Substrate Kit and images were acquired using the ChemiDoc Chemiluminescence Imaging System, and quantification was performed using ImageJ software.

Neonatal bacterial challenge and tissue collection for gene expression

Group B *Streptococcus* (GBS, CNCTC 10/84, serotype V, sequence type 26, from Dr. Thomas Hooven lab (82)) was originally isolated from a neonate with sepsis. From an overnight culture, a sub-culture was placed with fresh Tryptic Soy Broth (Cat# 211825; BD Bioscience, Franklin Lakes, NJ, USA) and grown to the logarithmic phase (OD600 0.8-0.9). Additional dilution was performed using sterile 1X PBS to reach working concentrations.

Thriving term neonates (14-16 days old) born to dams that did not receive any treatment and dams injected solely with HMGB1, PBS (vehicle for M2 MΦ) followed by HMGB1, or M2 MΦ followed by HMGB1 were intraperitoneally injected with $2x10^6$ colony-forming units of GBS in 200 µL 1X sterile PBS. Survivability, body weight, and rectal temperature of the challenged neonates were checked at 4-6 h intervals throughout the daytime for 5 days. A separate cohort of neonates born to dams that received M2 MΦ or PBS followed by HMGB1 were sacrificed at 14 days of life and the lung and intestine were preserved in RNA*later* Stabilization Solution for gene expression analysis (see "**RNA isolation, cDNA synthesis, and qPCR analysis of murine tissues**" above).

Neonatal tissue collection for gut microbiome analysis

Thriving neonates born to dams injected with HMGB1 and treated with vehicle or M2 MΦ were euthanized on post-natal day 14. Samples from the neonatal small intestine, cecum, and colon as well as environmental controls were obtained using sterile swabs (FLOQSwabs, Cat# 553C Copan Diagnostics, Murieta, CA, USA) under aseptic conditions. All swab samples collected for 16S rRNA gene sequencing were stored at -80°C until DNA extractions were performed.

DNA extraction

Genomic DNA was extracted from swabs of the small intestine, cecum, and colon (n = 20 each) and negative blank DNA extraction kit controls (n = 12) using the DNeasy PowerLyzer Powersoil kit (Qiagen, Germantown, MD, USA), with minor modifications to the manufacturer's protocol as previously described (83-85). All swabs were randomized across extraction runs. The purified DNA was stored at -20°C.

16s rRNA Gene Sequencing

The V4 region of the 16S rRNA gene was amplified and sequenced via the dual indexing strategy developed by Kozich et al. (86) as previously described (83-85, 87), with the exception that library builds were performed using 32 cycles of PCR prior to the equimolar pooling of all sample libraries for multiplex sequencing. 16S rRNA gene sequences were clustered into amplicon sequence variants (ASVs) defined by 100% sequence similarity using DADA2 version 1.12 (88) in R version 4.2.2 (89) as previously described (90), with the exception that forward and reverse reads were truncated at 240 and 215 bases, respectively. Sequences were then classified using the silva_nr_v132_train_set database with a minimum bootstrap value of 80%, and sequences that were derived from Archaea, chloroplast, Eukaryota, or mitochondria were removed.

Potential background DNA contaminant ASVs were identified using the R package decontam version 1.18.0 (91) and the "IsContaminant" function. One of the 82 ASVs identified as a contaminant (Lachnospiraceae_ASV2) was present in > 90% of both biological and control samples, however, it had a greater mean relative abundance in biological (12.95%) than in control samples (1.77%) and was therefore not removed from the dataset. The two taxa with the highest mean prevalence and abundance in control samples that were removed from the dataset were Burkholderiaceae_ASV42 (41.7% and 5.3%) and *Pseudomonas*_ASV97 (50.0% and 3.8%,

respectively). The mean relative abundances of these two ASVs across all biological samples were 0.0003% and 0.006%, respectively. Other ASVs removed from the dataset included taxa that have previously been reported to be contaminants in 16S rRNA gene sequencing studies (e.g., *Acinetobacter*, *Cloacibacterium*, *Corynebacterium*, *Cutibacterium*, *Escherichia*, *Halomonas*, *Pseudomonas*, *Ralstonia*, *Sphingomonas*, *Staphylococcus*, *Stenotrophomonas*, and *Xanthomonas*) (87, 92-95).

After removing contaminant ASVs, all samples were normalized to 8,715 reads using the "rarefy_even_depth" function in phyloseq 1.42.0 (96), resulting in 20 bacterial profiles with Good's coverage (97) values ≥ 99.68% for each of the three sample types. The final dataset contained a total of 411 ASVs. No cross-tissue comparisons were conducted.

Beta diversity

Beta diversity of bacterial profiles was characterized using the Bray-Curtis similarity index. Principal coordinate analysis (PCoA) plots were used to visualize the Bray-Curtis similarity of the sample profiles. Using nonparametric multivariate analysis of variance (NPMANOVA) as implemented in vegan 2.6.4 (98), differences in bacterial community structure across treatments were evaluated for each tissue type.

Differential abundance of bacterial species

Differential abundance of the 25 most prevalent ASVs between treatment groups was independently evaluated for the small intestine, cecum, and colon datasets using Mann-Whitney U-tests with Holm's correction for multiple comparisons as implemented in R version 4.2.2. Adjusted p-values < 0.1 were considered significant.

Statistics

Statistical analyses were performed using GraphPad Prism (v9.5.0; GraphPad, San Diego, CA, US) as indicated in each figure caption. Flow cytometry analysis was performed using FlowJo software version 10. Protein expression quantification was performed using ImageJ software. To determine gene expression levels from qPCR arrays, $-\Delta C_T$ values were calculated using averaged reference genes (*Actb, Gapdh, Gusb*, and *Hsp90ab1*) within each sample. Heatmaps were created to represent the Z-scores. Microbiome data analysis was performed using R (v.4.2.2; https://www.r-project.org/), as described above. A p-value ≤ 0.05 or adjusted p-value (q-value) ≤ 0.1 was considered statistically significant.

Study approval

All procedures were approved by the Institutional Animal Care and Use Committee (IACUC) at Wayne State University under Protocol Nos. A-07-03-15, 18-03-0584, and 21-04-3506.

Data availability

16S rRNA gene sequencing files and associated metadata have been uploaded to the National Center for Biotechnology Information's Sequence Read Archive (PRJNA925285). All other data are presented within the current manuscript and/or its supplementary materials.

Author contributions

Conceptualization: N.G.-L.

Methodology: V.G.-F., Z.L., Y.X., N.G.-L.

Validation: V.G.-F., Z.L., Y.X., N.G.-L.

Formal analysis: V.G.-F., Z.L., R.R., Y.X., J.G., A.D.W., M.F.-J., N.G.-L.

Investigation: V.G.-F., Z.L., Y.X., D.M., J.G., A.D.W., M.F.-J., N.G.-L.

Resources: R.R., K.R.T., N.G.-L.

Data curation: V.G.-F., Z.L., Y.X., A.D.W.

Writing – original draft: V.G.-F., D.M., J.G., N.G.-L.

Writing – review & editing: V.G.-F., Z.L., R.R., Y.X., D.M., J.G., A.D.W., M.F.-J., K.R.T., N.G.-L.

Visualization: V.G.-F., Z.L., J.G., A.D.W., N.G.-L.

Supervision: R.R., K.R.T., N.G.-L.

Project administration: N.G.-L.

Funding acquisition: R.R., N.G.-L.

Acknowledgements

This research was supported by the Perinatology Research Branch, Division of Obstetrics and Maternal-Fetal Medicine, Division of Intramural Research, *Eunice Kennedy Shriver* National Institute of Child Health and Human Development, National Institutes of Health, U.S. Department of Health and Human Services (NICHD/NIH/DHHS) under Contract No. HHSN275201300006C. This research was also supported by the Wayne State University Perinatal Initiative in Maternal, Perinatal and Child Health. R.R. has contributed to this work as part of his official duties as an employee of the United States Federal Government. The funders had no role in study design, data collection and interpretation, or the decision to submit the work for publication. Figures include art created with BioRender.com

REFERENCES

1. Liu L, et al. Global, regional, and national causes of child mortality in 2000-13, with projections to inform post-2015 priorities: an updated systematic analysis. *Lancet.* 2015;385(9966):430-440.
2. Guo X, et al. A birth population-based survey of preterm morbidity and mortality by gestational age. *BMC Pregnancy Childbirth.* 2021;21(1):291.
3. Romero R, et al. Preterm labor: one syndrome, many causes. *Science.* 2014;345(6198):760-765.
4. Goldenberg RL, et al. Epidemiology and causes of preterm birth. *Lancet.* 2008;371(9606):75-84.
5. Bastek JA, et al. The role of inflammation and infection in preterm birth. *Clin Perinatol.* 2011;38(3):385-406.
6. Yoon BH, et al. Clinical significance of intra-amniotic inflammation in patients with preterm labor and intact membranes. *Am J Obstet Gynecol.* 2001;185(5):1130-1136.
7. Romero R, et al. Prevalence and clinical significance of sterile intra-amniotic inflammation in patients with preterm labor and intact membranes. *Am J Reprod Immunol.* 2014;72(5):458-474.
8. Combs CA, et al. Amniotic fluid infection, inflammation, and colonization in preterm labor with intact membranes. *Am J Obstet Gynecol.* 2014;210(2):125.e121-125.e115.
9. Romero R, et al. Evidence of perturbations of the cytokine network in preterm labor. *Am J Obstet Gynecol.* 2015;213(6):836.e831-836.e818.
10. Bhatti G, et al. Compartmentalized profiling of amniotic fluid cytokines in women with preterm labor. *PLoS One.* 2020;15(1):e0227881.
11. Matzinger P. An innate sense of danger. *Semin Immunol.* 1998;10(5):399-415.
12. Rubartelli A, and Lotze MT. Inside, outside, upside down: damage-associated molecular-pattern molecules (DAMPs) and redox. *Trends Immunol.* 2007;28(10):429-436.
13. Romero R, et al. Damage-associated molecular patterns (DAMPs) in preterm labor with intact membranes and preterm PROM: a study of the alarmin HMGB1. *J Matern Fetal Neonatal Med.* 2011;24(12):1444-1455.
14. Gomez-Lopez N, et al. Intra-Amniotic Administration of HMGB1 Induces Spontaneous Preterm Labor and Birth. *Am J Reprod Immunol.* 2016;75(1):3-7.
15. Galaz J, et al. Betamethasone as a potential treatment for preterm birth associated with sterile intra-amniotic inflammation: a murine study. *J Perinat Med.* 2021;49(7):897-906.
16. Galaz J, et al. Clarithromycin prevents preterm birth and neonatal mortality by dampening alarmin-induced maternal-fetal inflammation in mice. *BMC Pregnancy Childbirth.* 2022;22(1):503.
17. Gomez-Lopez N, et al. Inflammasomes: Their Role in Normal and Complicated Pregnancies. *J Immunol.* 2019;203(11):2757-2769.
18. Gomez-Lopez N, et al. Inhibition of the NLRP3 inflammasome can prevent sterile intra-amniotic inflammation, preterm labor/birth, and adverse neonatal outcomes. *Biol Reprod.* 2019;100(5):1306-1318.
19. Motomura K, et al. The alarmin interleukin-1α causes preterm birth through the NLRP3 inflammasome. *Mol Hum Reprod.* 2020;26(9):712-726.

20. Motomura K, et al. RNA Sequencing Reveals Distinct Immune Responses in the Chorioamniotic Membranes of Women with Preterm Labor and Microbial or Sterile Intra-amniotic Inflammation. *Infect Immun.* 2021;89(5).
21. Galaz J, et al. A key role for NLRP3 signaling in preterm labor and birth driven by the alarmin S100B. *Transl Res.* 2023.
22. Cohen PE, et al. Macrophages: important accessory cells for reproductive function. *J Leukoc Biol.* 1999;66(5):765-772.
23. Repnik U, et al. Comparison of macrophage phenotype between decidua basalis and decidua parietalis by flow cytometry. *Placenta.* 2008;29(5):405-412.
24. Houser BL, et al. Two unique human decidual macrophage populations. *J Immunol.* 2011;186(4):2633-2642.
25. Svensson J, et al. Macrophages at the fetal-maternal interface express markers of alternative activation and are induced by M-CSF and IL-10. *J Immunol.* 2011;187(7):3671-3682.
26. Care AS, et al. Macrophages regulate corpus luteum development during embryo implantation in mice. *J Clin Invest.* 2013;123(8):3472-3487.
27. Svensson-Arvelund J, et al. The human fetal placenta promotes tolerance against the semiallogeneic fetus by inducing regulatory T cells and homeostatic M2 macrophages. *J Immunol.* 2015;194(4):1534-1544.
28. Xu Y, et al. An M1-like Macrophage Polarization in Decidual Tissue during Spontaneous Preterm Labor That Is Attenuated by Rosiglitazone Treatment. *J Immunol.* 2016;196(6):2476-2491.
29. Gomez-Lopez N, et al. Macrophages exert homeostatic actions in pregnancy to protect against preterm birth and fetal inflammatory injury. *JCI Insight.* 2021;6(19).
30. Qiu X, et al. Colony-stimulating factor-1-dependent macrophage functions regulate the maternal decidua immune responses against Listeria monocytogenes infections during early gestation in mice. *Infect Immun.* 2009;77(1):85-97.
31. Gomez-Lopez N, et al. The immunobiology of preterm labor and birth: intra-amniotic inflammation or breakdown of maternal-fetal homeostasis. *Reproduction.* 2022;164(2):R11-r45.
32. Lee J, et al. A new antibiotic regimen treats and prevents intra-amniotic inflammation/infection in patients with preterm PROM. *J Matern Fetal Neonatal Med.* 2016;29(17):2727-2737.
33. Oh KJ, et al. Evidence that antibiotic administration is effective in the treatment of a subset of patients with intra-amniotic infection/inflammation presenting with cervical insufficiency. *Am J Obstet Gynecol.* 2019;221(2):140 e141-140 e118.
34. Yoon BH, et al. Antibiotic administration can eradicate intra-amniotic infection or intra-amniotic inflammation in a subset of patients with preterm labor and intact membranes. *Am J Obstet Gynecol.* 2019;221(2):142 e141-142 e122.
35. Kacerovsky M, et al. Antibiotic administration reduces the rate of intraamniotic inflammation in preterm prelabor rupture of the membranes. *Am J Obstet Gynecol.* 2020;223(1):114 e111-114 e120.
36. Andreesen R, et al. Adoptive immunotherapy of cancer using monocyte-derived macrophages: rationale, current status, and perspectives. *J Leukoc Biol.* 1998;64(4):419-426.

37. Chernykh ER, et al. Safety and Therapeutic Potential of M2 Macrophages in Stroke Treatment. *Cell Transplant.* 2016;25(8):1461-1471.
38. Poltavets AS, et al. Macrophage Modification Strategies for Efficient Cell Therapy. *Cells.* 2020;9(6).
39. Motomura K, et al. Fetal and maternal NLRP3 signaling is required for preterm labor and birth. *JCI Insight.* 2022;7(16).
40. Gomez-Lopez N, et al. A Role for the Inflammasome in Spontaneous Preterm Labor With Acute Histologic Chorioamnionitis. *Reprod Sci.* 2017;24(10):1382-1401.
41. Gomez-Lopez N, et al. Inflammasome activation during spontaneous preterm labor with intra-amniotic infection or sterile intra-amniotic inflammation. *Am J Reprod Immunol.* 2018;80(5):e13049.
42. Gomez-Lopez N, et al. Gasdermin D: Evidence of pyroptosis in spontaneous preterm labor with sterile intra-amniotic inflammation or intra-amniotic infection. *Am J Reprod Immunol.* 2019;82(6):e13184.
43. Romero R, et al. The preterm labor syndrome. *Ann N Y Acad Sci.* 1994;734:414-429.
44. Norwitz ER, et al. The control of labor. *N Engl J Med.* 1999;341(9):660-666.
45. Romero R, et al. The preterm parturition syndrome. *Bjog.* 2006;113 Suppl 3(Suppl 3):17-42.
46. Smith R. Parturition. *N Engl J Med.* 2007;356(3):271-283.
47. Faro J, et al. Intra-amniotic inflammation induces preterm birth by activating the NLRP3 inflammasome. *Biol Reprod.* 2019;100(5):1290-1305.
48. Willcockson AR, et al. Transcriptome signature identifies distinct cervical pathways induced in lipopolysaccharide-mediated preterm birth. *Biol Reprod.* 2018;98(3):408-421.
49. Mittal P, et al. Characterization of the myometrial transcriptome and biological pathways of spontaneous human labor at term. *J Perinat Med.* 2010;38(6):617-643.
50. Pique-Regi R, et al. A single-cell atlas of the myometrium in human parturition. *JCI Insight.* 2022;7(5).
51. Garcia-Flores V, et al. A single-cell atlas of murine reproductive tissues during preterm labor. *Cell Rep.* 2022:111846.
52. Saito H, et al. Effects of aging on mortality, hypothermia, and cytokine induction in mice with endotoxemia or sepsis. *Mech Ageing Dev.* 2003;124(10-12):1047-1058.
53. Copeland S, et al. Acute inflammatory response to endotoxin in mice and humans. *Clin Diagn Lab Immunol.* 2005;12(1):60-67.
54. Migale R, et al. Modeling hormonal and inflammatory contributions to preterm and term labor using uterine temporal transcriptomics. *BMC Med.* 2016;14(1):86.
55. Pique-Regi R, et al. Single cell transcriptional signatures of the human placenta in term and preterm parturition. *Elife.* 2019;8.
56. Motomura K, et al. Pregnancy-specific transcriptional changes upon endotoxin exposure in mice. *J Perinat Med.* 2020;48(7):700-722.
57. Toothaker JM, et al. Immune Cells in the Placental Villi Contribute to Intra-amniotic Inflammation. *Front Immunol.* 2020;11:866.
58. Lavin Y, and Merad M. Macrophages: gatekeepers of tissue integrity. *Cancer Immunol Res.* 2013;1(4):201-209.
59. Roszer T. Understanding the Mysterious M2 Macrophage through Activation Markers and Effector Mechanisms. *Mediators Inflamm.* 2015;2015:816460.

60. Motomura K, et al. The alarmin S100A12 causes sterile inflammation of the human chorioamniotic membranes as well as preterm birth and neonatal mortality in mice. *Biol Reprod.* 2021;105(6):1494-1509.
61. Coll RC, et al. A small-molecule inhibitor of the NLRP3 inflammasome for the treatment of inflammatory diseases. *Nat Med.* 2015;21(3):248-255.
62. Shapouri-Moghaddam A, et al. Macrophage plasticity, polarization, and function in health and disease. *J Cell Physiol.* 2018;233(9):6425-6440.
63. Reisenberger K, et al. The transfer of interleukin-8 across the human placenta perfused in vitro. *Obstet Gynecol.* 1996;87(4):613-616.
64. Zaretsky MV, et al. Transfer of inflammatory cytokines across the placenta. *Obstet Gynecol.* 2004;103(3):546-550.
65. Dahlgren J, et al. Interleukin-6 in the maternal circulation reaches the rat fetus in mid-gestation. *Pediatr Res.* 2006;60(2):147-151.
66. Ponzio NM, et al. Cytokine levels during pregnancy influence immunological profiles and neurobehavioral patterns of the offspring. *Ann N Y Acad Sci.* 2007;1107:118-128.
67. Gershater M, et al. IL-22 Plays a Dual Role in the Amniotic Cavity: Tissue Injury and Host Defense against Microbes in Preterm Labor. *J Immunol.* 2022;208(7):1595-1615.
68. Gomez-Lopez N, et al. Regulatory T Cells Play a Role in a Subset of Idiopathic Preterm Labor/Birth and Adverse Neonatal Outcomes. *Cell Rep.* 2020;32(1):107874.
69. Gomez de Aguero M, et al. The maternal microbiota drives early postnatal innate immune development. *Science.* 2016;351(6279):1296-1302.
70. Lim AI, et al. Prenatal maternal infection promotes tissue-specific immunity and inflammation in offspring. *Science.* 2021;373(6558).
71. Mirabella F, et al. Prenatal interleukin 6 elevation increases glutamatergic synapse density and disrupts hippocampal connectivity in offspring. *Immunity.* 2021;54(11):2611-2631 e2618.
72. Cuna A, et al. Dynamics of the preterm gut microbiome in health and disease. *Am J Physiol Gastrointest Liver Physiol.* 2021;320(4):G411-G419.
73. Tamburini S, et al. The microbiome in early life: implications for health outcomes. *Nat Med.* 2016;22(7):713-722.
74. Ficara M, et al. Changes of intestinal microbiota in early life. *J Matern Fetal Neonatal Med.* 2020;33(6):1036-1043.
75. Puri K, et al. Association of Chorioamnionitis with Aberrant Neonatal Gut Colonization and Adverse Clinical Outcomes. *PLoS One.* 2016;11(9):e0162734.
76. Galaz J, et al. A Protocol for Evaluating Vital Signs and Maternal-Fetal Parameters Using High-Resolution Ultrasound in Pregnant Mice. *STAR Protoc.* 2020;1(3):100134.
77. Gomez-Lopez N, et al. In vivo T-cell activation by a monoclonal alphaCD3epsilon antibody induces preterm labor and birth. *Am J Reprod Immunol.* 2016;76(5):386-390.
78. St Louis D, et al. Invariant NKT Cell Activation Induces Late Preterm Birth That Is Attenuated by Rosiglitazone. *J Immunol.* 2016;196(3):1044-1059.
79. Meyer N, et al. High Frequency Ultrasound for the Analysis of Fetal and Placental Development In Vivo. *J Vis Exp.* 2018(141).
80. Arenas-Hernandez M, et al. Effector and Activated T Cells Induce Preterm Labor and Birth That Is Prevented by Treatment with Progesterone. *J Immunol.* 2019;202(9):2585-2608.
81. Arenas-Hernandez M, et al. Isolation of Leukocytes from the Murine Tissues at the Maternal-Fetal Interface. *J Vis Exp.* 2015(99):e52866.

82. Hooven TA, et al. Complete Genome Sequence of Streptococcus agalactiae CNCTC 10/84, a Hypervirulent Sequence Type 26 Strain. *Genome Announc.* 2014;2(6).
83. Theis KR, et al. No Consistent Evidence for Microbiota in Murine Placental and Fetal Tissues. *mSphere.* 2020;5(1).
84. Theis KR, et al. Lack of Evidence for Microbiota in the Placental and Fetal Tissues of Rhesus Macaques. *mSphere.* 2020;5(3).
85. Winters AD, et al. Does the Amniotic Fluid of Mice Contain a Viable Microbiota? *Front Immunol.* 2022;13:820366.
86. Kozich JJ, et al. Development of a dual-index sequencing strategy and curation pipeline for analyzing amplicon sequence data on the MiSeq Illumina sequencing platform. *Appl Environ Microbiol.* 2013;79(17):5112-5120.
87. Winters AD, et al. Does the endometrial cavity have a molecular microbial signature? *Sci Rep.* 2019;9(1):9905.
88. Callahan BJ, et al. DADA2: High-resolution sample inference from Illumina amplicon data. *Nat Methods.* 2016;13(7):581-583.
89. Team RC. R: A language and environment for statistical computing. 2013.
90. Romero R, et al. The vaginal microbiota in early pregnancy identifies a subset of women at risk for early preterm prelabor rupture of membranes and preterm birth. *Research Square.* 2022.
91. Davis NM, et al. Simple statistical identification and removal of contaminant sequences in marker-gene and metagenomics data. *Microbiome.* 2018;6(1):226.
92. Salter SJ, et al. Reagent and laboratory contamination can critically impact sequence-based microbiome analyses. *BMC Biol.* 2014;12:87.
93. Glassing A, et al. Inherent bacterial DNA contamination of extraction and sequencing reagents may affect interpretation of microbiota in low bacterial biomass samples. *Gut Pathog.* 2016;8:24.
94. Eisenhofer R, et al. Contamination in Low Microbial Biomass Microbiome Studies: Issues and Recommendations. *Trends Microbiol.* 2019;27(2):105-117.
95. Karstens L, et al. Controlling for Contaminants in Low-Biomass 16S rRNA Gene Sequencing Experiments. *mSystems.* 2019;4(4).
96. McMurdie PJ, and Holmes S. phyloseq: an R package for reproducible interactive analysis and graphics of microbiome census data. *PLoS One.* 2013;8(4):e61217.
97. Good IJ. The population frequencies of species and the estimation of population parameters. *Biometrika.* 1953;40(3-4):237-264.
98. Dixon P. VEGAN, a package of R functions for community ecology. *Journal of Vegetation Science.* 2003;14(6):927-930.

Figures and Figure Legends

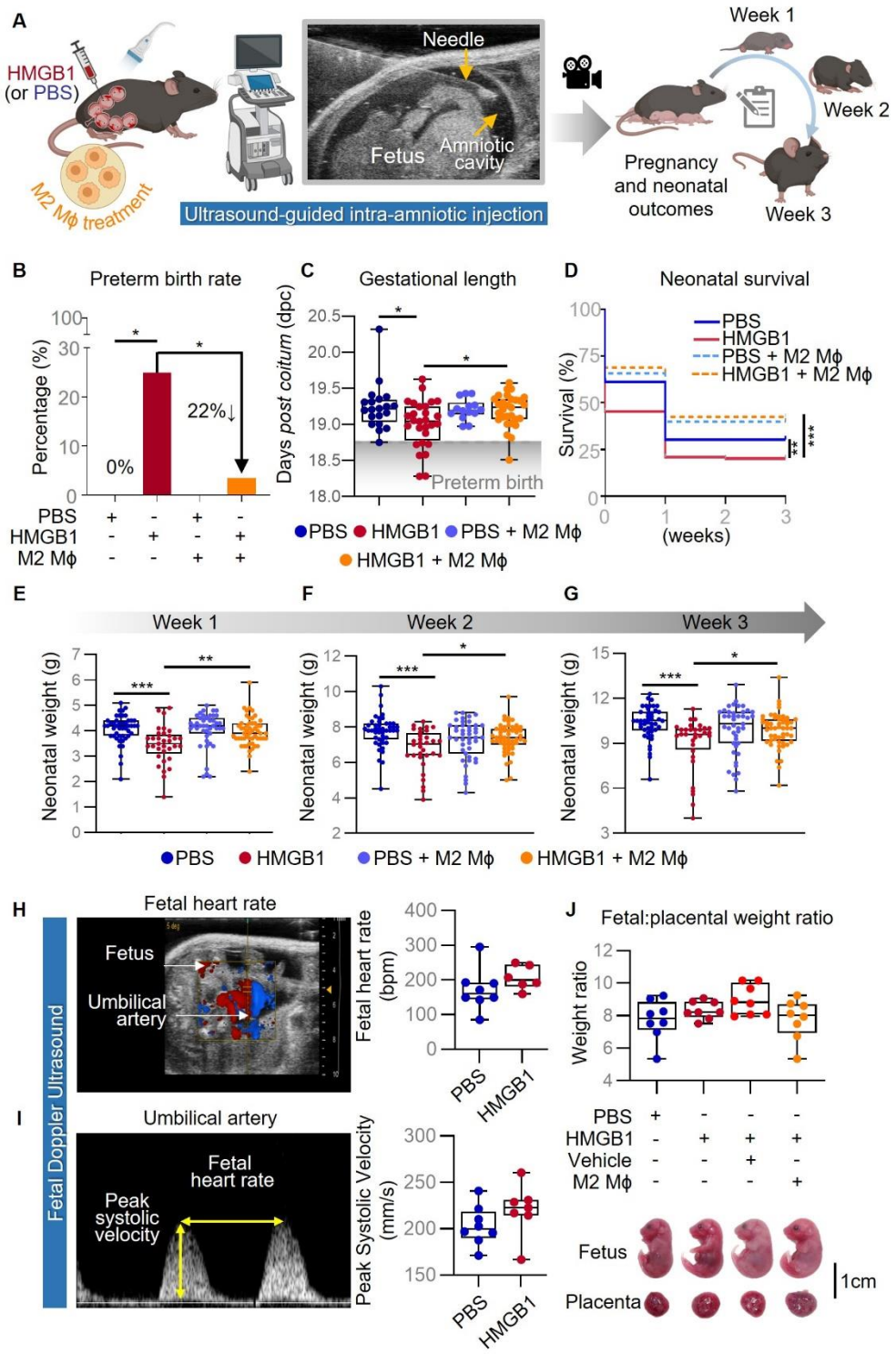

Figure 1. Adoptive transfer of M2-polarized macrophages prevents HMGB1-induced preterm birth and improves neonatal outcomes. (A) Bone marrow-derived cells were collected

from the C57BL/6 mice, differentiated, and polarized to an M2 phenotype (M2 MΦ) *in vitro*. M2 MΦ were administered intravenously to C57BL/6 dams on 13.5 days *post coitum* (dpc) and 14.5 dpc followed by ultrasound-guided intra-amniotic injection of HMGB1 (or PBS as control) on 14.5 dpc. Dams were monitored until delivery, and neonatal survival and weight were recorded until three weeks of age. **(B)** Rates of preterm birth among dams injected with PBS (n = 20), HMGB1 (n = 28), PBS + M2 MΦ (n = 14), and HMGB1 + M2 MΦ (n = 29) are shown as bar plots. P-values were determined using Fisher's exact test. **(C)** Gestational length shown as box plots where midlines indicate medians and whiskers indicate minimum/maximum range. P-values were determined using the Kruskal-Wallis test followed by two-stage linear step-up procedure of Benjamini, Krieger, and Yekutieli post-hoc test. **(D)** Kaplan-Meier survival curves from neonates at weeks 1, 2, and 3 of life. PBS (n = 20 litters), HMGB1 (n = 20 litters), PBS + M2 MΦ (n = 14 litters), and HMGB1 + M2 MΦ (n = 16 litters). P-values were determined using the Gehan-Breslow-Wilcoxon test. **(E-G)** Individual weights (g) of neonates across the first three weeks of life are shown as box plots where midlines indicate medians and whiskers indicate minimum/maximum range. PBS (n = 11 litters), HMGB1 (n = 11 litters), PBS + M2 MΦ (n = 11 litters), and HMGB1 + M2 MΦ (n = 14 litters). P-values were determined using the Kruskal-Wallis test followed by Dunn's post-hoc test. **(H-I)** Representative images of high-resolution Doppler ultrasound of the umbilical artery used to determine the **(H)** fetal heart rate and **(I)** umbilical artery peak systolic velocity in dams that received PBS (n = 8) or HMGB1 (n = 6-7) at 96 h post-injection. Data are shown as box plots where midlines indicate medians and whiskers indicate minimum/maximum range. P-values were determined using the Mann-Whitney U-test. **(J)** The fetal:placental weight ratio at 72 h post-injection (n = 8 per group). Representative images show a fetus and placenta from each group. Scale bar represents 1 cm. Data are shown as box plots where midlines indicate medians and whiskers indicate minimum/maximum range. P-values were determined using the Mann-Whitney U-test. *$p < 0.05$; **$p < 0.01$; ***$p < 0.001$.

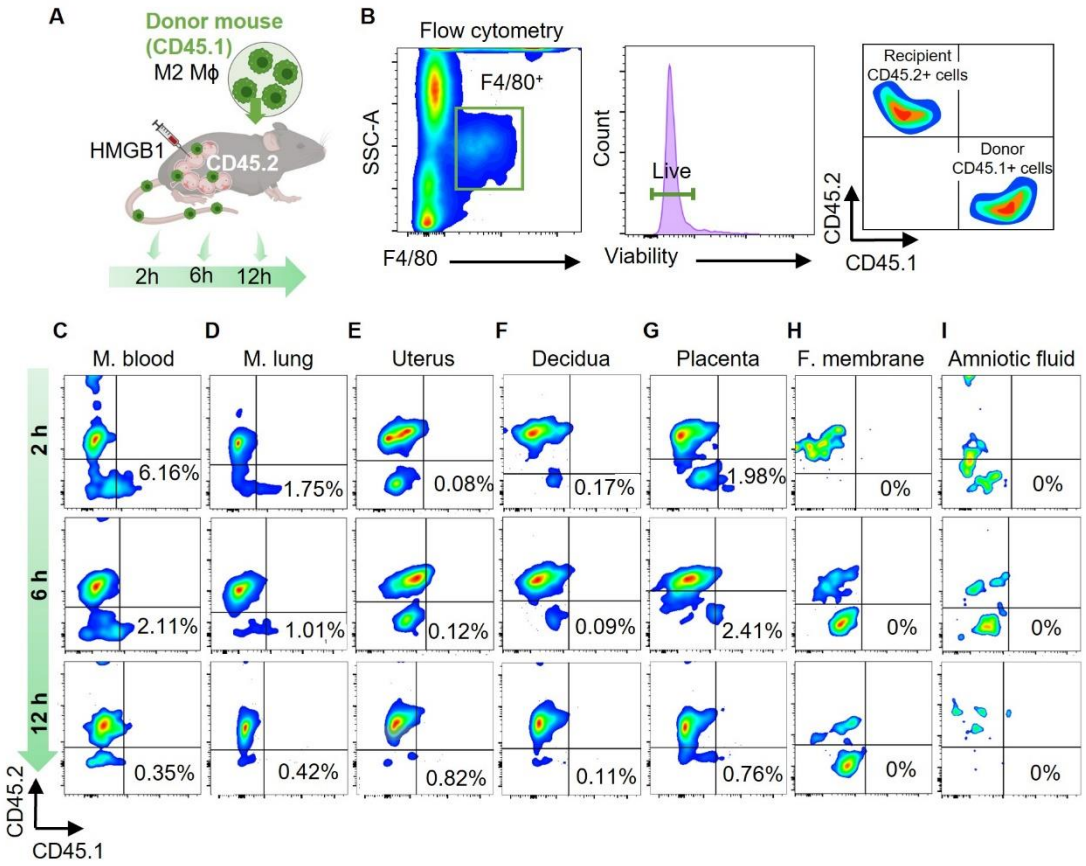

Figure 2. Adoptively transferred M2-polarized macrophages reach maternal compartments and the maternal-fetal interface. (A) Bone marrow-derived cells were collected from donor CD45.1^{+} mice, differentiated, and polarized to donor M2 MΦ *in vitro*. Donor M2 MΦ were intravenously administered on 13.5 days *post coitum* (dpc) and 14.5 dpc to recipient CD45.2^{+} dams followed by intra-amniotic injection of HMGB1 on 14.5 dpc. Maternal and fetal tissues were collected at 2, 6, or 12 h post-HMGB1 injection (n = 1 dam per time point) to track donor M2 macrophage infiltration. **(B)** Representative gating strategy for detection of live CD45.1^{+}F4/80^{+} or CD45.2^{+}F4/80^{+} cells. **(C-I)** Representative flow cytometry plots to detect CD45.1^{+}CD45.2^{-} donor macrophages in the **(C)** maternal blood, **(D)** maternal lung, **(E)** uterus, **(F)** decidua, **(G)** placenta, **(H)** fetal membrane, and **(I)** amniotic fluid of recipient dams at 2 (top row), 6 (middle row), or 12 (bottom row) h post-HMGB1 injection. Proportions of donor macrophages are shown in the bottom right corner of each plot.

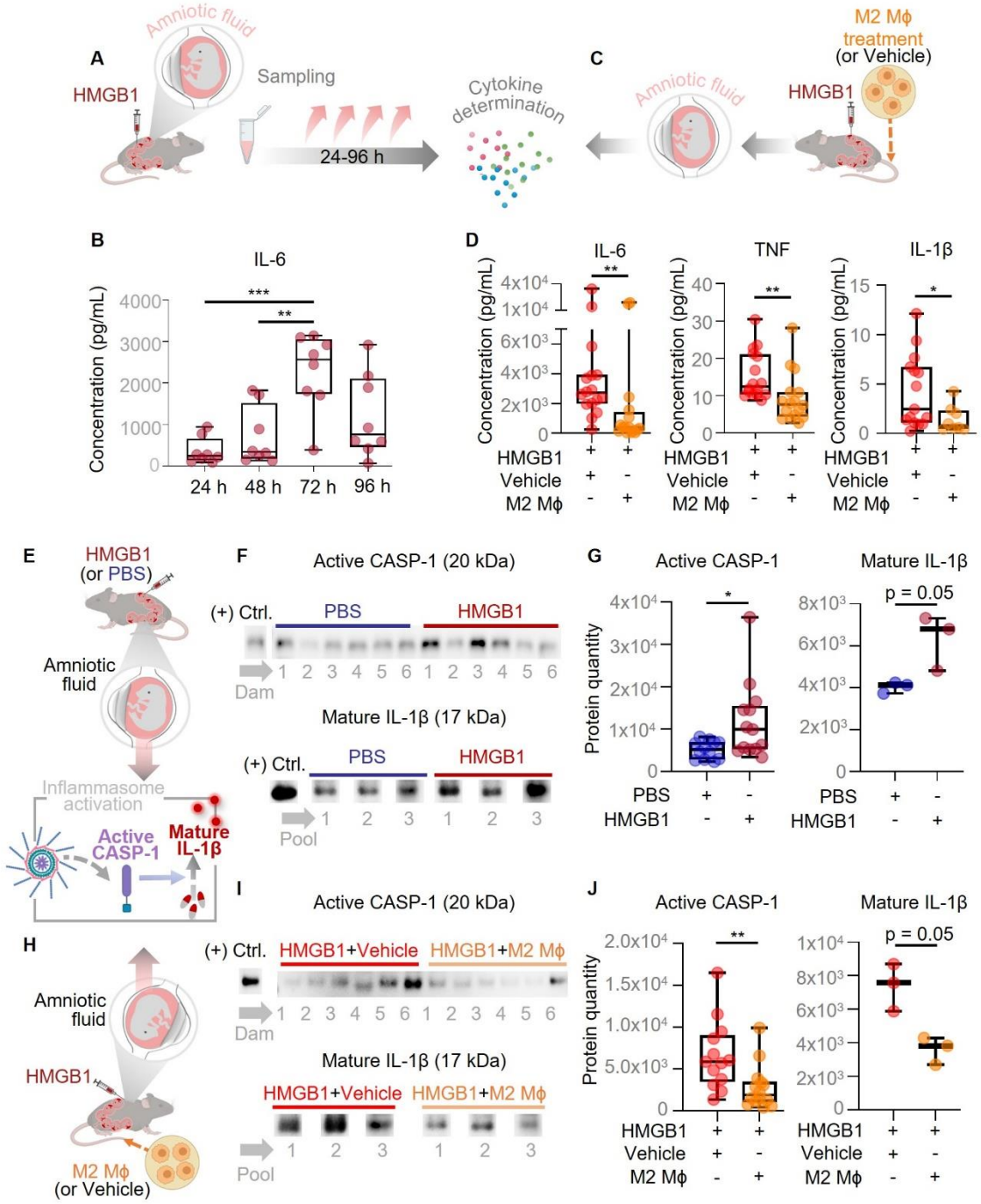

Figure 3. M2-polarized macrophages reduce HMGB1-induced inflammation and inflammasome activation in the amniotic cavity. (A) Dams were intra-amniotically injected with HMGB1 on 14.5 days *post coitum* (dpc). Amniotic fluid was collected at 24, 48, 72, or 96 h post-HMGB1 injection for cytokine determination. **(B)** Concentrations of IL-6 in the amniotic fluid of HMGB1-injected dams at 24, 48, 72, and 96 h post-injection are shown as box plots (n = 8 dams per time point). P-values were determined using the Kruskal-Wallis test followed by two-stage linear step-up procedure of Benjamini, Krieger, and Yekutieli post-hoc test. **(C)** M2-

polarized macrophages (M2 MΦ) or vehicle (PBS) were intravenously administered on 13.5 dpc and 14.5 dpc to dams followed by ultrasound-guided intra-amniotic injection of HMGB1 on 14.5 dpc. Amniotic fluid was collected at 72 h post-HMGB1 injection for cytokine determination. **(D)** The concentrations of IL-6, TNF, and IL-1β in the amniotic fluid of the Vehicle+HMGB1 dams (n = 16 dams) or M2 MΦ+HMGB1 dams (n = 16 dams) at 72 h post-injection are shown as box plots. P-values were determined using the Mann-Whitney U-test. **(E)** Amniotic fluid of dams that received intra-amniotic PBS or HMGB1 was collected at 72 h post-HMGB1 injection for immunoblotting. **(F)** Immunoblotting of active CASP-1 expression and mature IL-1β expression in the amniotic fluid of dams injected with PBS or HMGB1. Representative CASP-1 immunoblot image shows 6 samples per group, and representative mature IL-1β immunoblot image shows 3 pooled samples (pooled amniotic fluids from 3 dams) per group. **(G)** Protein quantification of active CASP-1 in the amniotic fluid of dams injected with PBS (n = 12) or HMGB1 (n = 13). Protein quantification of mature IL-1β in the pooled amniotic fluid of dams injected with PBS (n = 3) or HMGB1 (n = 3). Data are shown as box plots. P-values were determined using the Mann-Whitney U-test or t-test. **(H)** Amniotic fluid of dams that received intra-amniotic HMGB1 followed by administration of M2 MΦ or vehicle control was collected at 72 h post-HMGB1 injection for immunoblotting. **(I)** Immunoblotting of active CASP-1 expression mature IL-1β expression in the amniotic fluid of Vehicle+HMGB1 or M2 MΦ+HMGB1 dams. Representative CASP-1 immunoblot image shows 6 samples per group, and representative mature IL-1β immunoblot image shows 3 pooled samples (pooled amniotic fluids from 3 dams) per group. **(J)** Protein quantification of active CASP-1 in the amniotic fluid of dams injected with PBS (n = 12) or HMGB1 (n = 14). Protein quantification of mature IL-1β in the pooled amniotic fluid of dams injected with PBS (n = 3) or HMGB1 (n = 3). P-values were determined using the Mann-Whitney U-test or t-test. Data are shown as boxplots where midlines indicate medians, boxes denote interquartile ranges, and whiskers indicate the minimum/maximum range. *$p < 0.05$; **$p < 0.01$; ***$p < 0.001$.

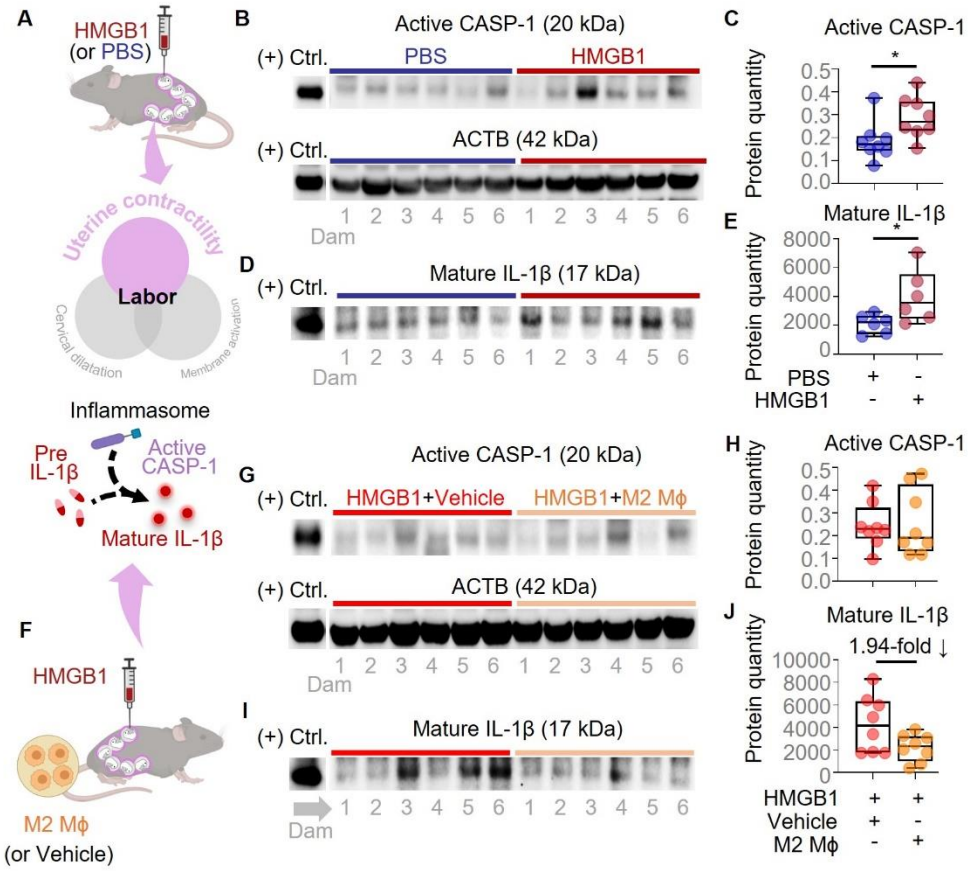

992

993 **Figure 4. M2-polarized macrophages dampen HMGB1-induced inflammasome activation in**
994 **the uterus. (A)** Dams received intra-amniotic injection of PBS (control) or HMGB1 on 14.5 days
995 *post coitum* (dpc). The uterus was collected at 72 h post-HMGB1 injection for immunoblotting.
996 **(B)** Immunoblotting of active CASP-1 and β-actin (ACTB) expression in the uterine tissues from
997 PBS- or HMGB1-injected dams. Representative immunoblot images depict 6 samples per group
998 in each gel. **(C)** Protein quantification of active CASP-1 (normalized by ACTB) in the uterus of
999 PBS- or HMGB1-injected dams (n = 8 per group). **(D)** Immunoblotting of mature IL-1β expression
1000 in the uterus following immunoprecipitation with anti-IL-1β antibody. The representative
1001 immunoblot image depicts 6 samples per group. **(E)** Protein quantification of mature IL-1β in the
1002 uterus of PBS- or HMGB1-injected dams (n = 6 per group). **(F)** M2-polarized macrophages (M2
1003 MΦ) or vehicle (PBS) were intravenously administered to dams on 13.5 dpc and 14.5 dpc followed
1004 by intra-amniotic injection of HMGB1 on 14.5 dpc. The uterus was collected at 72 h post-HMGB1
1005 injection for immunoblotting. **(G)** Immunoblotting of active CASP-1 and β-actin (ACTB)
1006 expression in the uterine tissues from Vehicle+M2 MΦ or HMGB1+M2 MΦ dams. Representative
1007 immunoblot images depict 6 samples per group in each gel. **(H)** Protein quantification of active
1008 CASP-1 (normalized by ACTB) in the uterus of Vehicle+M2 MΦ or HMGB1+M2 MΦ dams (n
1009 = 8 per group). **(I)** Immunoblotting of mature IL-1β expression in the uterus following
1010 immunoprecipitation with anti-IL-1β antibody. The representative immunoblot image depicts 6
1011 samples per group. **(J)** Protein quantification of mature IL-1β in the uterus of Vehicle+M2 MΦ or

HMGB1+M2 MΦ dams (n = 8 per group). P-values were determined using the Mann-Whitney U-test. Data are shown as boxplots where midlines indicate medians, boxes denote interquartile ranges, and whiskers indicate the minimum/maximum range. *$p < 0.05$.

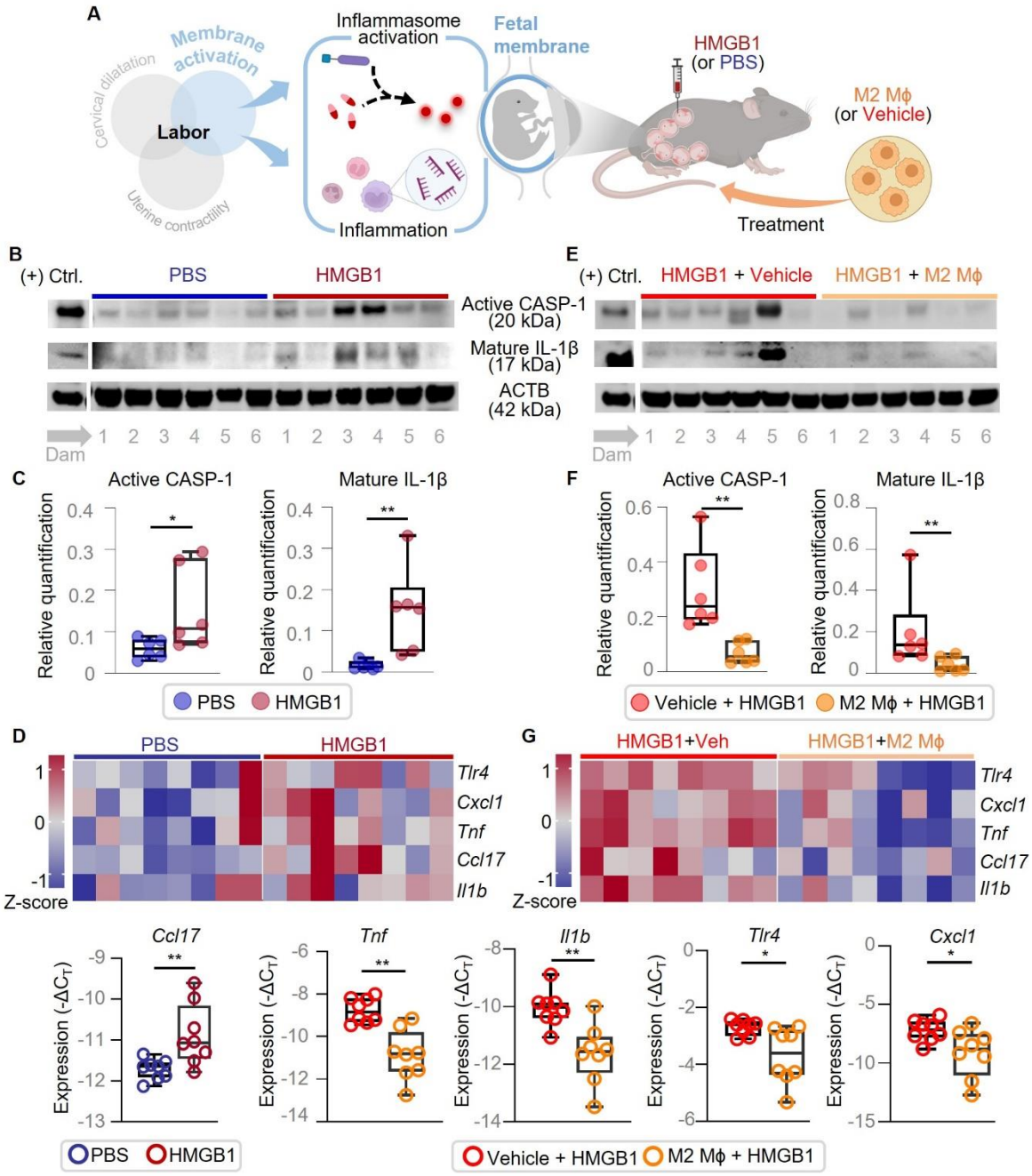

Figure 5. M2-polarized macrophages dampen the HMGB1-induced inflammatory response in the fetal membranes. (A) Dams received intra-amniotic injection of PBS (control) or HMGB1 on 14.5 days *post coitum* (dpc). M2-polarized macrophages (M2 MΦ) or vehicle (PBS) were intravenously administered to dams on 13.5 dpc and 14.5 dpc followed by intra-amniotic injection of HMGB1 on 14.5 dpc. Tissue collection was performed at 72 h post-injection to collect the fetal membranes for immunoblotting and determination of gene expression. **(B)** Immunoblotting of active CASP-1, mature IL-1β, and β-actin (ACTB) in the fetal membranes from PBS- or HMGB1-injected dams. Representative immunoblot images depict 6 samples per group in each gel. **(C)**

Protein quantification of active CASP-1 and mature IL-1β (both normalized by ACTB) in the fetal membranes of PBS- or HMGB1-injected dams (n = 6 per group). **(D)** Representative heatmaps displaying the expression of key inflammatory genes in the fetal membranes of PBS- (n = 8) or HMGB1-injected (n = 8) dams. Expression of *Ccl17* in the fetal membranes of PBS- or HMGB1-injected dams. Data are shown as boxplots where midlines indicate medians, boxes denote interquartile ranges, and whiskers indicate the minimum/maximum range. P-values were determined using the Mann-Whitney U-test. **(E)** Immunoblotting of active CASP-1, mature IL-1β, and β-actin (ACTB) in the fetal membranes from HMGB1+Vehicle or HMGB1+M2 MΦ dams. Representative immunoblot images depict 6 samples per group in each gel. **(F)** Relative quantification of active CASP-1 and mature IL-1β (both normalized by ACTB) in the fetal membranes of HMGB1+Vehicle or HMGB1+M2 MΦ dams (n = 6 per group). **(G)** Representative heatmaps displaying the expression of key inflammatory genes in the fetal membranes of HMGB1+Vehicle (n = 8) or HMGB1+M2 MΦ (n = 8) dams. Expression of *Tnf, Il1b, Tlr4*, and *Cxcl1* in the fetal membranes of HMGB1+Vehicle or HMGB1+M2 MΦ dams. Data are shown as boxplots where midlines indicate medians, boxes denote interquartile ranges, and whiskers indicate the minimum/maximum range. P-values were determined using the Mann-Whitney U-test. *$p < 0.05$; **$p < 0.01$.

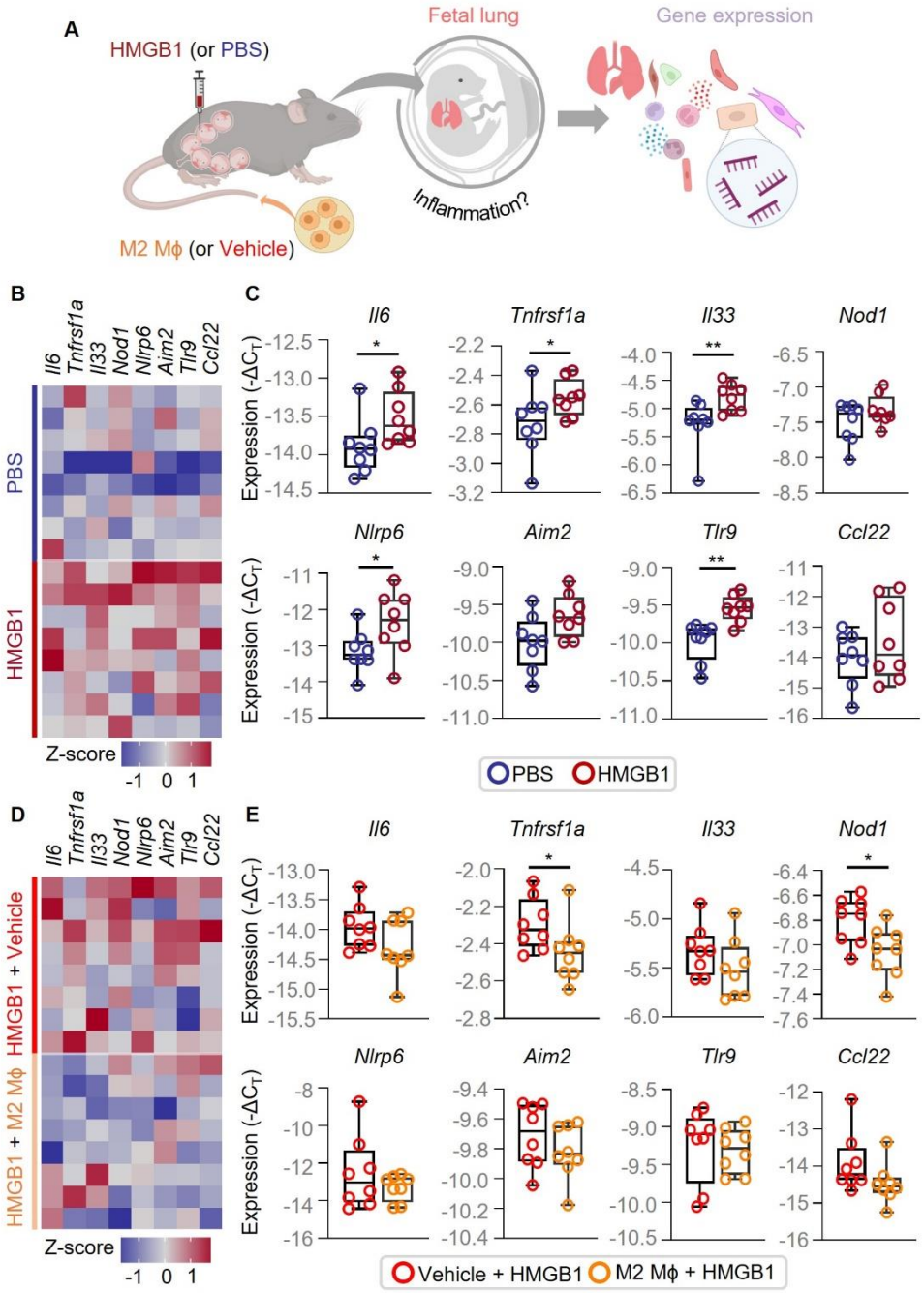

Figure 6. M2-polarized macrophages reduce HMGB1-induced inflammation in the fetal lung. (A) Dams received intra-amniotic injection of PBS (control) or HMGB1 on 14.5 days *post coitum* (dpc). M2-polarized macrophages (M2 MΦ) or vehicle (PBS) were intravenously administered to dams on 13.5 dpc and 14.5 dpc followed by intra-amniotic injection of HMGB1 on 14.5 dpc. Tissue collection was performed at 72 h post-injection to collect the fetal lung for gene expression. **(B)** Representative heatmaps displaying the expression of inflammatory genes in the fetal lung of PBS- (n = 8) or HMGB1-injected (n = 8) dams. **(C)** Expression of *Il6*, *Tnfrsf1a*, *Il33*, *Nod1*, *Nlrp6*, *Aim2*, *Tlr9*, and *Ccl22* in the fetal lung of PBS- or HMGB1-injected dams. Data

are shown as boxplots where midlines indicate medians, boxes denote interquartile ranges, and whiskers indicate the minimum/maximum range. P-values were determined using the Mann-Whitney U-test. **(D)** Representative heatmaps displaying the expression of inflammatory genes in the fetal lung of HMGB1+Vehicle (n = 8) or HMGB1+M2 MΦ (n = 8) dams. **(E)** Expression of *Il6*, *Tnfrsf1a*, *Il33*, *Nod1*, *Nlrp6*, *Aim2*, *Tlr9*, and *Ccl22* in the fetal lung of HMGB1+Vehicle or HMGB1+M2 MΦ dams. Data are shown as boxplots where midlines indicate medians, boxes denote interquartile ranges, and whiskers indicate the minimum/maximum range. P-values were determined using the Mann-Whitney U-test. *$p < 0.05$; **$p < 0.01$.

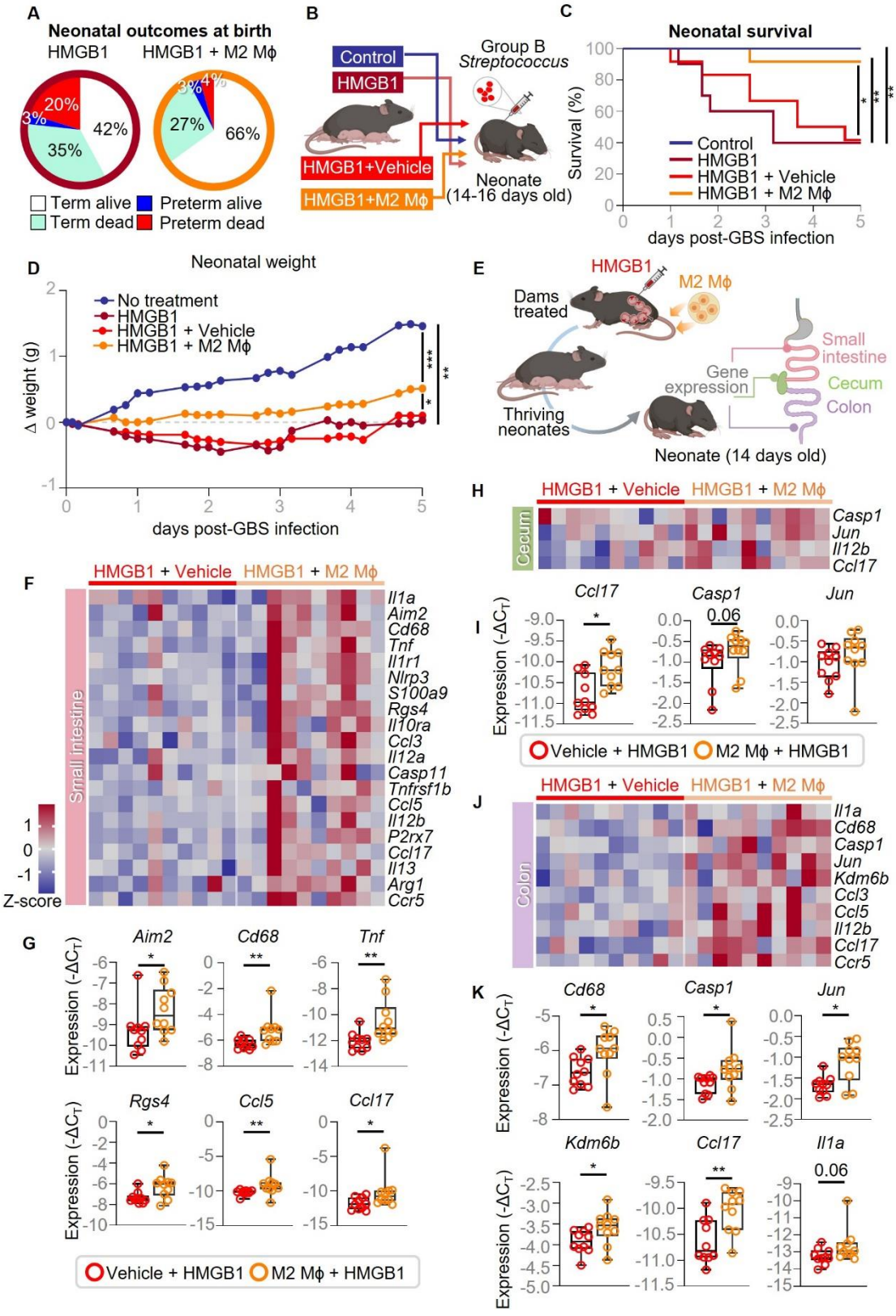
A
Neonatal outcomes at birth
HMGB1
HMGB1 + M2 Mϕ
20%
3%
42%
35%
3%
4%
27%
66%
Term alive
Preterm alive
Term dead
Preterm dead
B
Control
HMGB1
HMGB1+Vehicle
HMGB1+M2 Mϕ
Group B Streptococcus
Neonate (14-16 days old)
C
Neonatal survival
Survival (%)
Control
HMGB1
HMGB1 + Vehicle
HMGB1 + M2 Mϕ
days post-GBS infection
D
Neonatal weight
No treatment
HMGB1
HMGB1 + Vehicle
HMGB1 + M2 Mϕ
Δ weight (g)
days post-GBS infection
E
HMGB1
M2 Mϕ
Dams treated
Thriving neonates
Gene expression
Small intestine
Cecum
Colon
Neonate (14 days old)
F
HMGB1 + Vehicle
HMGB1 + M2 Mϕ
Small intestine
Il1a
Aim2
Cd68
Tnf
Il1r1
Nlrp3
S100a9
Rgs4
Il10ra
Ccl3
Il12a
Casp11
Tnfrsf1b
Ccl5
Il12b
P2rx7
Ccl17
Il13
Arg1
Ccr5
Z-score
G
Aim2
Cd68
Tnf
Rgs4
Ccl5
Ccl17
Expression (-ΔC_T)
Vehicle + HMGB1
M2 Mϕ + HMGB1
H
HMGB1 + Vehicle
HMGB1 + M2 Mϕ
Cecum
Casp1
Jun
Il12b
Ccl17
I
Ccl17
Casp1
Jun
0.06
Expression (-ΔC_T)
Vehicle + HMGB1
M2 Mϕ + HMGB1
J
HMGB1 + Vehicle
HMGB1 + M2 Mϕ
Colon
Il1a
Cd68
Casp1
Jun
Kdm6b
Ccl3
Ccl5
Il12b
Ccl17
Ccr5
K
Cd68
Casp1
Jun
Kdm6b
Ccl17
Il1a
0.06
Expression (-ΔC_T)

1058

Figure 7. M2-polarized macrophages restore neonatal immunocompetence following *in utero* exposure to HMGB1. (A) Neonatal outcomes at birth displayed as proportions (white = term delivery and born alive; light blue = term delivery and born dead; dark blue = preterm delivery and born alive; red = preterm delivery and born dead). PBS (n = 20 litters), HMGB1 (n = 20 litters), PBS + M2 MΦ (n = 14 litters), and HMGB1 + M2 MΦ (n = 16 litters). **(B)** M2-polarized macrophages (M2 MΦ) or vehicle (PBS) were intravenously administered to dams on 13.5 dpc and 14.5 dpc followed by intra-amniotic injection of HMGB1 on 14.5 dpc. Pregnant dams without any treatment or injected with HMGB1 alone were also included. After delivery, thriving neonates were monitored until 14-16 days of age, after which they received intraperitoneal injection of group B *Streptococcus* (GBS) and were observed for five days. **(C)** The survival rates of GBS-infected neonates born to untreated (n = 10 neonates), HMGB1-injected (n = 10 neonates), HMGB1+Vehicle (n = 12 neonates), or HMGB1+M2 MΦ (n = 12 neonates) dams over the five days post-challenge are displayed as Kaplan-Meier survival curves. P-values were determined using the Gehan-Breslow-Wilcoxon test. **(D)** Mean weights of GBS-infected neonates over the five days post-challenge. P-values for comparing the mean weight at the end of day five (final data point in plot) were determined using the Mann-Whitney U-test. **(E-J)** A separate group of dams received M2 MΦ or vehicle followed by HMGB1 and were allowed to deliver. The neonatal small intestine, cecum, and colon were collected at 14 days of life to determine gene expression. Representative heatmaps display gene expression in the **(F)** neonatal small intestine, **(H)** cecum, and **(J)** colon of neonates born to HMGB1+Vehicle (n = 10 neonates) or HMGB1+M2 MΦ (n = 10 neonates) dams. The expression of specific genes in the **(G)** neonatal small intestine, **(I)** cecum, and **(K)** colon are shown as box plots. P-values were determined using the Mann-Whitney U-test. Data are shown as boxplots where midlines indicate medians, boxes denote interquartile ranges, and whiskers indicate the minimum/maximum range. *$p < 0.05$; **$p < 0.01$; ***$p < 0.001$.

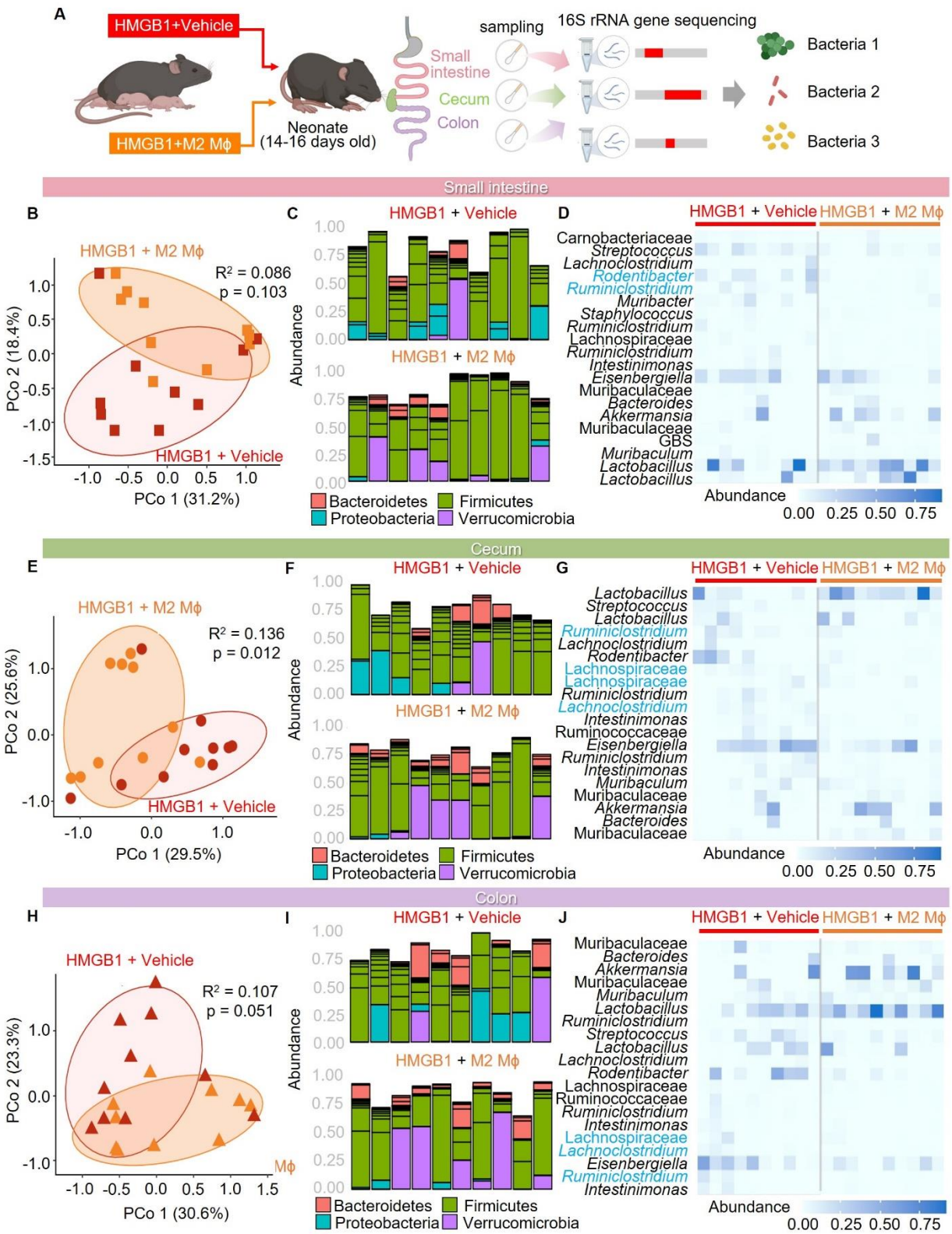

Figure 8. M2-polarized macrophages restore the neonatal microbiome following *in utero* exposure to HMGB1. (A) M2-polarized macrophages (M2 MΦ) or vehicle (PBS) were

intravenously administered to dams on 13.5 dpc and 14.5 dpc followed by intra-amniotic injection of HMGB1 on 14.5 dpc. After delivery, neonates were monitored until 14-16 days of age, after which the small intestine, cecum, and colon were collected for microbial analysis using 16S rRNA gene sequencing (n = 10 neonates per group). Principal coordinates (PC) analysis illustrating variation in the 16S rRNA gene profiles among the **(B)** small intestine, **(E)** cecum, and **(H)** colon. Similarities in the 16S rRNA gene profiles were characterized using the Bray-Curtis similarity index. Bar plots showing the taxonomic classifications of the 20 bacterial taxa with highest relative abundance across all **(C)** small intestine, **(F)** cecum, and **(I)** colon samples. Multiple taxa with the same bacterial taxonomic classification within a same sample are indicated by bars of the same color. Heatmap displaying the relative abundance and taxonomy of the 20 most relatively abundant bacterial taxa among the 16S rRNA gene profiles of **(D)** small intestine, **(G)** cecum, and **(J)** colon samples. Bacterial taxa with significantly altered abundance between groups are labelled in blue in the heatmaps. P-values were determined using Mann-Whitney U-tests with Holm's correction for multiple comparisons.